

Deeply-Learned Generalized Linear Models with Missing Data

David K. Lim

Department of Biostatistics, University of North Carolina at Chapel Hill
and

Naim U. Rashid

Department of Biostatistics, University of North Carolina at Chapel Hill
and

Junier B. Oliva

Department of Computer Science, University of North Carolina at Chapel Hill
and

Joseph G. Ibrahim

Department of Biostatistics, University of North Carolina at Chapel Hill

July 20, 2022

Abstract

Deep Learning (DL) methods have dramatically increased in popularity in recent years, with significant growth in their application to supervised learning problems in the biomedical sciences. However, the greater prevalence and complexity of missing data in modern biomedical datasets present significant challenges for DL methods. Here, we provide a formal treatment of missing data in the context of deeply learned generalized linear models, a supervised DL architecture for regression and classification problems. We propose a new architecture, *dlglm*, that is one of the first to be able to flexibly account for both ignorable and non-ignorable patterns of missingness in input features and response at training time. We demonstrate through statistical simulation that our method outperforms existing approaches for supervised learning tasks in the presence of missing not at random (MNAR) missingness. We conclude with a case study of a Bank Marketing dataset from the UCI Machine Learning Repository, in which we predict whether clients subscribed to a product based on phone survey data.

Keywords: missing data, supervised learning, deeply learned glm, MNAR

1 Introduction

Deep Learning (DL) methods have been increasingly used in an array of supervised learning problems in various fields, especially in the biomedical sciences (Razzak et al. 2017, Lopez et al. 2018). While a number of deep learning architectures have been proposed for supervised learning, the feed forward neural network (FFNN) is very commonly used in most architectures. In a FFNN, sequential non-linear transformations are applied to the values of the input layer. Each value in the subsequent layer of the FFNN is computed by applying a non-linear (or “activation”) function to the linear transformation of the values in the previous layer, outputting a complex non-linear transformation of the input (Svozil et al. 1997). For example, a FFNN architecture called deeply-learned GLM (Tran et al. 2019) has been applied in the context of supervised learning to describe nonlinear relationships between the covariates and the response. These networks may contain a large number of parameters and take a long time to train, so optimization is often done via stochastic gradient descent, for scalability (Guo & Gelfand 1990).

However, the common presence of missing data in biomedical datasets can hinder the training and generalizability of supervised deep learning methods (Wells et al. 2013), where missingness can occur both in the input features and the response variable. Missingness has commonly been categorized into three mechanisms: Missing Completely At Random (MCAR), Missing At Random (MAR), and Missing Not At Random (MNAR) (Rubin 1976). While a number of methods have been proposed in the statistical literature to address MNAR missingness in the regression setting (Ibrahim et al. 2005), such methods often cannot take into account complex relationships between predictors and response and are not scalable to higher dimensions (Chen et al. 2019), or have been specifically designed for unsupervised learning tasks (Lim et al. 2021). Supervised deep learning is one way to address capture complex relationships between predictors and response in a scalable manner (Kingma & Welling 2019), however it is unclear how best to account for more complex forms of missingness, such as MAR or MNAR missingness, in this setting.

There have been some recent attempts to perform prediction using deep learning in the presence of missing features (Ipsen et al. 2021), but such methods typically assume

either MCAR or MAR missingness. Commonly used methods in supervised deep learning such as mean imputation or complete case analysis have historically yielded biased results (Ibrahim & Molenberghs 2009). Multiple Imputation by Chained Equations (*mice*) has also been widely employed to handle missing data in a supervised learning setting, but *mice* is unable to apply a trained imputation model to handle missingness that may exist at test time (Hoogland et al. 2020). In addition, multiple imputation-based methods may not be feasible to apply when the downstream model is computationally intensive, such as in the setting of training a deep learning neural network, since one must train the model separately for each imputed dataset. Moreover, existing approaches to handle MAR or MCAR missingness when training deep learning models for supervised learning tasks are currently limited, and have not been sufficiently explored in the literature.

To address these issues, we present *dlglm*: a deep generalized linear model (GLM) for probabilistic supervised learning in the presence of missing input features and/or response across a variety of missingness patterns. Our proposed method utilizes variational inference to learn approximate posterior distributions for the missing variables, and replaces missing entries with samples from these distributions during maximization. In this way, *dlglm* can perform supervised learning in the presence of missingness in both the features and the response of interest. We also incorporate a model for the missingness, which can take into account MNAR patterns of missingness, even at training time. Through neural networks, *dlglm* is able to model complex non-linear relationships between the input features and the response, and is scalable to large quantities and dimensionalities of data. In addition, we can achieve interpretability of our learned neural network by exactly modelling a GLM, utilizing an assumed distributional family for the response variable, and an appropriate link function to describe its relationship with the covariates, allowing us to perform coefficient estimation, like in a traditional GLM. After training the *dlglm* architecture, prediction can be done seamlessly on fully- or partially-observed samples using the trained model, without requiring separate imputation of the missing values.

2 Methods

Here we first discuss the formulation of the generalized linear model (GLM) in Section 2.1, and then introduce the deeply-learned GLM in Section 2.2. We then discuss missingness in the context of GLMs in Section 2.3, and lastly propose a novel deep learning architecture *dlglm* in Section 2.4 to fit deeply learned GLMs in the presence of missingness.

2.1 Generalized Linear Models (GLMs)

Let \mathbf{X} be the $n \times p$ matrix of covariates (input features) with observation vectors \mathbf{x}_i , where each corresponding entry x_{ij} denotes the value of the i^{th} observation of the j^{th} feature for $i = 1, \dots, n$ and $j = 1, \dots, p$. Also, let $\mathbf{Y} = \{y_1, \dots, y_n\}$ be the vector of univariate responses where y_i is the response pertaining to the i^{th} observation. We note that y_i may also be assumed to be multivariate; however, we focus specifically on the case of univariate response to simplify the discussion, and discuss extensions to the setting of multivariate response in Section 4. Then, denote $\boldsymbol{\eta} = \mathbf{X}\boldsymbol{\beta}$, where $\boldsymbol{\beta}$ is a vector of regression coefficients and $\boldsymbol{\eta}$ is the linear predictor. Also define $\boldsymbol{\mu} = \{\mu_1, \dots, \mu_n\}$ with $\mu_i = E(y_i|\mathbf{x}_i)$ and link function $g(\cdot)$ such that $g(\mu_i) = \eta_i = \mathbf{x}_i\boldsymbol{\beta}$. We assume that the conditional distribution $p(y_i|\mathbf{x}_i)$ is a member of the exponential family of distributions (McCullagh & Nelder 2019), such that $p(y_i|\mathbf{x}_i)$ can be written as

$$p(y_i|\mathbf{x}_i) = \exp \left[\frac{y_i\Theta_i - b(\Theta_i)}{a(\alpha)} + c(y_i, \alpha) \right],$$

with canonical parameter Θ_i , dispersion parameter α , and some functions $a(\cdot)$, $b(\cdot)$, and $c(\cdot)$. Here, we further assume $g(\cdot)$ is a canonical link function such that $g(\mu_i) = \Theta_i$. With the appropriate specification of the canonical link $g(\cdot)$ and variance function $V_\alpha(\cdot)$, we obtain the formulation of a GLM.

GLMs were first motivated by the limitations of the traditional linear model, which imposed strict assumptions of linearity between $\boldsymbol{\mu}$ and \mathbf{X} and of normality of errors with fixed variance. GLMs instead utilize specific link and variance functions, allowing for model fitting on types of response data that may violate these assumptions, such as count or categorical outcomes, without having to rely on heuristic transformations of the data (Nelder & Wedderburn 1972). Typically, GLMs are estimated by utilizing iteratively re-

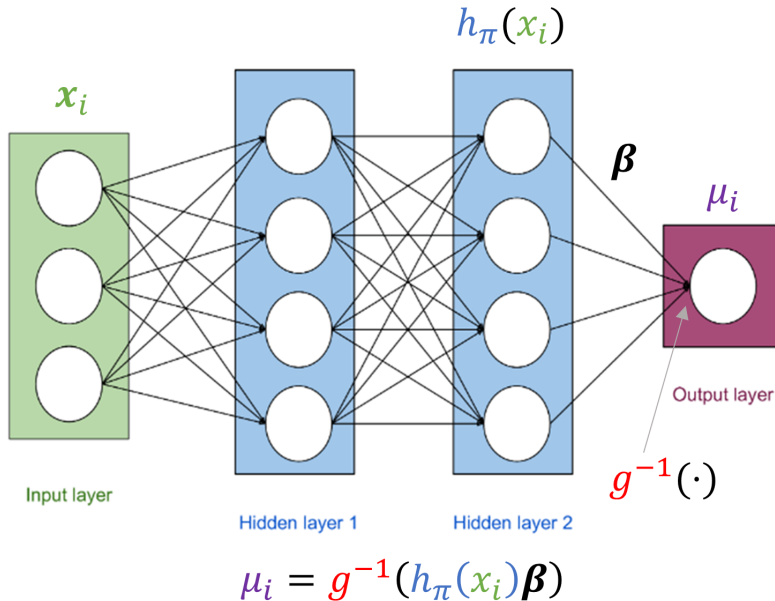


Figure 1: Visualization of a sample deeply-learned GLM architecture $s_{\pi,\beta}(\mathbf{x}_i)$. Here, π denotes the set of weights and biases pertaining to the portion of the architecture from the input layer to the second to last layer (hidden layer 2). $h_{\pi}(\mathbf{x}_i)$ is a subset of the entire architecture, such that $s_{\pi,\beta}(\mathbf{x}_i) = h_{\pi}(\mathbf{x}_i)\boldsymbol{\beta}$. Original artwork of a feed-forward neural network (Dormehl 2019) was modified to show deeply-learned GLM architecture.

weighted least squares in lower dimensions (Holland & Welsch 1977), with extensions to the higher dimensional case via penalized likelihood (Friedman et al. 2010).

2.2 Deeply Learned GLMs

The traditional GLM assumes $g(\mu_i)$ is a linear function of \mathbf{x}_i , i.e. $g(\mu_i) = \mathbf{x}_i\boldsymbol{\beta}$. In many modern applications, one may wish to model $g(\mu_i)$ as a non-linear function of \mathbf{x}_i or capture complex interactions between features to predict response (Qi & Wu 2003). In such cases, we may generalize the GLM to a deeply-learned GLM (Tran et al. 2019) with the following expression: $g(\mu_i) = \eta_i = h_{\pi}(\mathbf{x}_i)\boldsymbol{\beta}$, where $h_{\pi}(\cdot)$ denotes the output of a series of non-linear transformations applied to the input \mathbf{X} by a neural network, with weights and bias parameters denoted by π . In addition, η_i can alternatively be expressed $\eta_i = s_{\pi,\beta}(\mathbf{x}_i)$, where $s_{\pi,\beta}(\cdot)$ is a neural network where $\boldsymbol{\beta}$ denotes the weights and bias associated with the output (last) layer of $s_{\pi,\beta}(\cdot)$. This formulation allows for the traditional interpretation of $\boldsymbol{\beta}$ as the coefficients pertaining to a transformed version of the input covariates. Figure 1 shows an illustration of this architecture.

Let n_{HL} denote the number of hidden layers in $s_{\pi, \beta}(\cdot)$. We note that if $n_{HL} = 0$, then $h_{\pi}(\mathbf{x}_i) = \mathbf{x}_i$ and $s_{\beta}(\mathbf{x}_i) = \mathbf{x}_i \boldsymbol{\beta}$, reducing to the traditional GLM. In this setting, $\boldsymbol{\beta}$ pertains to the intercept and regression coefficients. Deeply learned GLMs and other neural networks are often maximized using stochastic gradient descent (Bottou 2012). Details of this algorithm can be found in Appendix A1 of the supplementary materials.

2.3 Missingness in GLMs

Modern biomedical datasets often contain complex forms of missingness (Ghorbani & Zou 2018). In GLMs, missingness can exist in either \mathbf{X} or \mathbf{Y} . Therefore, we specify three cases of missingness in this context: missing covariates with fully-observed response (*Case x*), missing response with fully-observed covariates (*Case y*), and missing covariates and missing response (*Case xy*). Define $\mathbf{R} = \{\mathbf{R}^X, \mathbf{R}^Y\}$ as the “missingness mask”, which denotes the missingness of $\{\mathbf{X}, \mathbf{Y}\}$, such that \mathbf{R}^X and \mathbf{R}^Y have the same dimension as \mathbf{X} and \mathbf{Y} , respectively, and a value of 1 in \mathbf{R} denotes that the corresponding entry in $\{\mathbf{X}, \mathbf{Y}\}$ is observed, while a value of 0 denotes that it is unobserved. Additionally, let $\mathbf{R} = \{\mathbf{r}_1, \dots, \mathbf{r}_n\}$ with $\mathbf{r}_i = \{\mathbf{r}_i^X, \mathbf{r}_i^Y\} = \{r_{i1}^X, \dots, r_{ip}^X, r_i^Y\}$, $\mathbf{R}^X = \{\mathbf{r}_1^X, \dots, \mathbf{r}_n^X\}$, and $\mathbf{R}^Y = \{\mathbf{r}_1^Y, \dots, \mathbf{r}_n^Y\}$ with elements \mathbf{r}_i^X and \mathbf{r}_i^Y pertaining to the missingness of the i^{th} observation of \mathbf{X} and \mathbf{Y} , respectively. Then, \mathbf{X} and \mathbf{Y} can be factored into the unobserved and observed entries $\{\mathbf{X}^m, \mathbf{X}^o\}$ and $\{\mathbf{Y}^m, \mathbf{Y}^o\}$, respectively, such that $\mathbf{X}^m = \{\mathbf{X} : \mathbf{R}^X = 0\}$ with $\mathbf{x}_i^m = \{\mathbf{x}_i : \mathbf{r}_i^X = 0\}$, $\mathbf{X}^o = \{\mathbf{X} : \mathbf{R}^X = 1\}$ with $\mathbf{x}_i^o = \{\mathbf{x}_i : \mathbf{r}_i^X = 1\}$, and $\mathbf{Y}^m = \{\mathbf{Y} : \mathbf{R}^Y = 0\}$ and $\mathbf{Y}^o = \{\mathbf{Y} : \mathbf{R}^Y = 1\}$, with $\mathbf{y}_i^m = \{\mathbf{y}_i : \mathbf{r}_i^Y = 0\}$ and $\mathbf{y}_i^o = \{\mathbf{y}_i : \mathbf{r}_i^Y = 1\}$.

Missingness was classified into three primary mechanisms in the seminal work by Little & Rubin (2002): missing completely at random (MCAR), missing at random (MAR), and missing not at random (MNAR). They satisfy the following relations:

- MCAR: $p(\mathbf{r}_i | \mathbf{x}_i, y_i, \boldsymbol{\phi}) = p(\mathbf{r}_i | \boldsymbol{\phi})$
- MAR: $p(\mathbf{r}_i | \mathbf{x}_i, y_i, \boldsymbol{\phi}) = p(\mathbf{r}_i | \mathbf{x}_i^o, y_i^o, \boldsymbol{\phi})$
- MNAR: $p(\mathbf{r}_i | \mathbf{x}_i, y_i, \boldsymbol{\phi}) = p(\mathbf{r}_i | \mathbf{x}_i^o, \mathbf{x}_i^m, y_i^o, y_i^m, \boldsymbol{\phi})$.

Here, $\boldsymbol{\phi}$ denotes the collection of parameters for the model of the missingness mask \mathbf{r}_i . In

the presence of missingness, the marginal log-likelihood can generally be written as

$$\begin{aligned} \log p_{\alpha, \beta, \pi, \psi, \phi}(\mathbf{X}^o, \mathbf{Y}^o, \mathbf{R}) &= \log \iint p_{\alpha, \beta, \pi, \psi, \phi}(\mathbf{X}, \mathbf{Y}, \mathbf{R}) d\mathbf{X}^m d\mathbf{Y}^m \\ &= \log \iint p_{\alpha, \beta, \pi}(\mathbf{Y}|\mathbf{X}) p_{\psi}(\mathbf{X}) p_{\phi}(\mathbf{R}|\mathbf{X}, \mathbf{Y}) d\mathbf{X}^m d\mathbf{Y}^m, \end{aligned} \quad (1)$$

where ψ is a set of parameters associated with the covariate distribution $p_{\psi}(\mathbf{X})$. We factor $p_{\alpha, \beta, \pi, \psi, \phi}(\mathbf{X}, \mathbf{Y}, \mathbf{R})$ using the selection model factorization (Diggle & Kenward 1994).

Under MNAR, it is not possible to remove $p_{\phi}(\mathbf{R}|\mathbf{X}, \mathbf{Y})$ from the integral, since \mathbf{R} can depend on $\{\mathbf{X}^m, \mathbf{Y}^m\}$. Therefore, MNAR missingness is said to be non-ignorable, because it requires specification of the so-called ‘‘missingness model’’ $p(\mathbf{r}_i|\mathbf{x}_i, y_i, \phi)$ (Stubbendick & Ibrahim 2003). There are a number of ways to specify this model. For example, Diggle & Kenward (1994) proposes a binomial model for the missing data mechanism, which can be written in this setting as

$$p(\mathbf{R}|\mathbf{X}, \mathbf{Y}, \phi_{j_m}) = \prod_{i=1}^n \prod_{j_m=1}^{p_{miss}} [p(r_{ij_m} = 1|\mathbf{x}_i, y_i, \phi_{j_m})]^{r_{ij_m}} [1 - p(r_{ij_m} = 1|\mathbf{x}_i, y_i, \phi_{j_m})]^{1-r_{ij_m}},$$

where $j_m = 1, \dots, p_{miss}$ indexes the p_{miss} features in $\{\mathbf{X}, \mathbf{Y}\}$ that contain missingness. Here $p_{miss} = p_{miss}^X + p_{miss}^Y$, where p_{miss}^X is the total number of features containing missingness in \mathbf{X} , and p_{miss}^Y is 1 if \mathbf{Y} contains missingness (0 otherwise). Also, ϕ_{j_m} is the set of coefficients pertaining to the missingness model of the j_m^{th} missing variable, and $p(r_{ij_m} = 1|\mathbf{x}_i, y_i, \phi_{j_m})$ can be modeled straightforwardly by a logistic regression model, such that

$$\text{logit}[p(r_{ij_m} = 1|\mathbf{x}_i, y_i, \phi_{j_m})] = \phi_{0j_m} + y_i \phi_{1j_m} + \mathbf{x}_i^o \phi_{2j_m} + \mathbf{x}_i^m \phi_{3j_m},$$

where ϕ_{0j_m} is the intercept of the j_m^{th} missingness model, ϕ_{1j_m} is the coefficient pertaining to the response variable \mathbf{Y} , and $\phi_{2j_m} = \{\phi_{2,j_m,1}, \dots, \phi_{2,j_m,p_{obs}^X}\}^T$ and $\phi_{3j_m} = \{\phi_{3,j_m,1}, \dots, \phi_{3,j_m,p_{miss}^X}\}^T$ are the sets of coefficients of the j_m^{th} variable’s missingness model pertaining to the effects of the observed and missing features on the missingness, respectively, with p_{obs}^X and p_{miss}^X denoting the number of completely-observed and partially observed features in \mathbf{X} , respectively. Note that this model assumes independence of \mathbf{R} across the p_{miss} missing features, such that the missingness of each variable is conditionally independent of whether any other variable has been observed, which may or may not be realistic in some settings (Ibrahim et al. 2005).

When missingness is assumed to be MAR or MCAR, the marginal log-likelihood can be factored as $\log p_{\alpha, \beta, \pi, \psi, \phi}(\mathbf{X}^o, \mathbf{Y}^o, \mathbf{R}) = \log p_{\alpha, \beta, \pi, \psi}(\mathbf{X}^o, \mathbf{Y}^o) + \log p_{\phi}(\mathbf{R}|\mathbf{X}^o, \mathbf{Y}^o)$. In this case, the quantity $\log p_{\phi}(\mathbf{R}|\mathbf{X}^o, \mathbf{Y}^o)$ need not be specified, since it is independent from the parameters of interest pertaining to $p_{\alpha, \beta, \pi, \psi}(\mathbf{X}^o, \mathbf{Y}^o)$. Therefore, MAR or MCAR missingness is often referred to as “ignorable” missingness. Equation (1) can then be expressed as

$$\log p_{\alpha, \beta, \pi, \psi}(\mathbf{X}^o, \mathbf{Y}^o) = \log \iint p_{\alpha, \beta, \pi}(\mathbf{Y}|\mathbf{X}) p_{\psi}(\mathbf{X}) d\mathbf{X}^m d\mathbf{Y}^m. \quad (2)$$

2.4 Deeply-learned GLM with Missingness (*dlglm*)

In this section, we propose an algorithm for training deeply-learned GLMs in the presence of MCAR, MAR, and MNAR missingness. Before discussing this model, we first discuss the specification of the so-called covariate distribution $p_{\psi}(\mathbf{X})$ introduced in Equations 1 and 2, which is critical for maximizing the marginal log-likelihood in either setting. In Sections 2.4.1-2.4.2, we discuss two different models for $p_{\psi}(\mathbf{X})$, and then in Section 2.4.3 we propose a novel method to handle missingness using a deeply-learned GLM architecture with an Importance-Weighted Autoencoder (IWAE) covariate structure. To simplify the discussion, we narrow the scope of our discussion to the *Case x* setting, where only \mathbf{X} contains missingness, but note that the proposed methodology naturally extends to *Case y* and *Case xy* settings as well.

2.4.1 Modeling $p_{\psi}(\mathbf{X})$ with known distribution

Given Eq. 1, we must model \mathbf{X} with some assumed covariate distribution $p_{\psi}(\mathbf{X})$. Care must be taken in specifying this distribution, as improper specification may reduce the accuracy of estimation of the parameters of interest β (Lipsitz & Ibrahim 1996). For example, we may assume $p_{\psi}(\mathbf{X})$ follows some known multivariate distribution such as the multivariate normal, where $\mathbf{X} \sim N_p(\boldsymbol{\mu}, \boldsymbol{\Sigma})$ and $\psi = \{\boldsymbol{\mu}, \boldsymbol{\Sigma}\}$. Here, ψ can be optimized jointly with the rest of the parameters $\{\alpha, \beta, \pi, \phi\}$ that are involved in the marginal log-likelihood. However, this assumption may not be applicable in many instances such as in the case when \mathbf{X} contains mixed data types, where both continuous and discrete features may be correlated and a joint distribution may be difficult to specify in closed form. In certain cases, it may be beneficial to model $p_{\psi}(\mathbf{X})$ flexibly, such that no strong prior assumptions

need to be made on the form of this distribution. To address this, a sequence of 1-D conditionals have previously been proposed to model the covariate distribution (Lipsitz & Ibrahim 1996), but such a model may be computationally intractable when the number of covariates is very large. Still, if an explicit form for the covariate distribution can be specified, a lower bound of the marginal log-likelihood in the presence of missingness, as introduced in Section 2.3, can be derived. This derivation can be found in Appendix A2 of the supplementary materials.

2.4.2 Modelling $p_\psi(\mathbf{X})$ with Variational and Importance-Weighted Autoencoders

Alternatively, one can approximately learn $p_\psi(\mathbf{X})$ from the training data by using an IWAE neural network architecture. In this section, we first introduce a general form of the variational autoencoder (VAE) and IWAE in the case of completely-observed data \mathbf{X} . Then, in Section 2.4.3, we apply the IWAE covariate structure to the deeply-learned GLM setting and show how this representation naturally extends to the case where MCAR, MAR, or MNAR missingness is observed in \mathbf{X} when training deeply-learned GLMs.

First, let \mathbf{Z} be an $n \times d$ matrix, such that $\mathbf{Z} = \{\mathbf{z}_1, \dots, \mathbf{z}_n\}$ and \mathbf{z}_i is a latent vector of length d pertaining to the i^{th} sample latent variable, and let \mathbf{Z} represent a lower-dimensional representation or subspace of \mathbf{X} . In a VAE, we assume $\mathbf{x}_1, \dots, \mathbf{x}_n$ are i.i.d. samples from a multivariate p.d.f or “generative model” $p_\psi(\mathbf{X}|\mathbf{Z})$ with accompanying parameters ψ that describes how \mathbf{X} is generated from the lower dimensional space \mathbf{Z} . In this manner, a VAE aims to learn accurate representations of high-dimensional data, and may be used to generate synthetic data with similar qualities as the training data. These aspects are also aided through the use of embedded deep learning neural networks, for example within $p_\psi(\mathbf{X}|\mathbf{Z})$, which also facilitates its applicability to larger dimensions and complex datasets.

In a VAE with completely observed training data, one aims to maximize the marginal log-likelihood as $\log p_\psi(\mathbf{X}) = \log \int p_\psi(\mathbf{X}, \mathbf{Z})d\mathbf{Z} = \log \int p_\psi(\mathbf{X}|\mathbf{Z})p(\mathbf{Z})d\mathbf{Z}$. However, due to the integral involved, this quantity is often intractable and is difficult to maximize directly. Therefore, VAE’s alternatively optimize the so-called “Evidence Lower Bound” (ELBO),

which lower bounds $\log p_\psi(\mathbf{X})$ and has the following form (Kingma & Welling 2013):

$$\mathcal{L}^{ELBO}(\theta, \psi) = \mathbb{E}_{\mathbf{Z} \sim q_\theta(\mathbf{Z}|\mathbf{X})} \log \left[\frac{p_\psi(\mathbf{X}|\mathbf{Z})p(\mathbf{Z})}{q_\theta(\mathbf{Z}|\mathbf{X})} \right] \quad (3)$$

$$\hat{\mathcal{L}}_K^{ELBO}(\theta, \psi) = \frac{1}{K} \sum_{k=1}^K \log \left[\frac{p_\psi(\mathbf{X}|\tilde{\mathbf{Z}}_k)p(\tilde{\mathbf{Z}}_k)}{q_\theta(\tilde{\mathbf{Z}}_k|\mathbf{X})} \right]. \quad (4)$$

Here, $\mathcal{L}^{ELBO}(\theta, \psi)$ denotes the ELBO such that $\mathcal{L}^{ELBO}(\theta, \psi) \leq \log p_\psi(\mathbf{X})$. Also let $\hat{\mathcal{L}}_K^{ELBO}(\theta, \psi)$ denote the empirical approximation to Eq. (3) computed by Monte Carlo integration, such that $\mathcal{L}^{ELBO}(\theta, \psi) \approx \hat{\mathcal{L}}_K^{ELBO}(\theta, \psi)$ and $\tilde{\mathbf{Z}}_1, \dots, \tilde{\mathbf{Z}}_K$ are K samples drawn from $q_\theta(\mathbf{Z}|\mathbf{X})$, the variational approximation of the true but intractable posterior $p_\psi(\mathbf{Z}|\mathbf{X})$, also called the ‘‘recognition model’’. Furthermore, denote $f_\psi(\mathbf{Z})$ and $g_\theta(\mathbf{X})$ as the decoder and encoder feed forward neural networks of the VAE, where ψ and θ are the sets of weights and biases pertaining to each of these neural networks, respectively. Given \mathbf{Z} , $f_\psi(\mathbf{Z})$ outputs the distributional parameters pertaining to $p_\psi(\mathbf{X}|\mathbf{Z})$.

In variational inference, $q_\theta(\mathbf{Z}|\mathbf{X})$ is constrained to be from a class of simple distributions, or ‘‘variational family’’, to obtain the best candidate from within that class to approximate $p_\psi(\mathbf{Z}|\mathbf{X})$. Variational inference is usually used in tandem with amortization of the parameters where the neural network parameters are shared across observations (Gershman & Goodman 2014), allowing for stochastic gradient descent (SGD) to be used for optimization of Eq. (4) (Kingma & Welling 2019). In practice, both $q_\theta(\mathbf{Z}|\mathbf{X})$ and $p(\mathbf{Z})$ are typically assumed to have simple forms, such as multivariate Gaussians with diagonal covariance structures, and $q_\theta(\mathbf{Z}|\mathbf{X})$ is commonly assumed to be factorizable, such that $q_\theta(\mathbf{Z}|\mathbf{X}) = \prod_{i=1}^n q_\theta(\mathbf{z}_i|\mathbf{x}_i)$ (Kingma & Welling 2019).

Let $(\hat{\theta}^{(t)}, \hat{\psi}^{(t)})$ be the estimates of (θ, ψ) at update (or iteration) t . For $t = 0$, these values are often initialized to small values centered around 0, although other initialization schemes may be used (Saxe et al. 2014, Murphy 2016). Each subsequent update $t \geq 1$ consists of two general steps to maximize $\mathcal{L}(\theta, \psi)$. First, K samples are drawn from $q_{\hat{\theta}^{(t)}}(\mathbf{Z}|\mathbf{X})$ to compute the quantity in Eq. (4), conditional on $\hat{\theta}^{(t)}$, similar to importance sampling. Then, the so-called ‘‘reparametrization trick’’ is utilized to facilitate the calculation of gradients of this approximation to obtain $(\hat{\theta}^{t+1}, \hat{\psi}^{t+1})$ using stochastic gradient descent (Kingma & Welling 2013). The networks $f_\psi(\mathbf{Z})$ and $g_\theta(\mathbf{X})$ also allow the VAE to capture complex and non-

linear relationships between features in outputting the distributional parameters for the generative and recognition models, respectively. This procedure may be repeated for a fixed number of iterations, or may be terminated early due to pre-specified convergence criteria (Prechelt 1998). Kingma & Welling (2013) provides additional details on the maximization procedure for VAEs.

The IWAE (Burda et al. 2015) is a generalization of the standard VAE. Both the VAE and IWAE estimate $\log p_\psi(\mathbf{X})$ by drawing samples of latent variables to estimate an expectation. However, while the VAE utilizes $p_\psi(\mathbf{X}, \mathbf{Z})/q_\theta(\mathbf{Z}|\mathbf{X})$ as the importance weights in deriving the ELBO, the IWAE uses the average of K importance weights in the integrand for a tighter lower bound of the marginal log-likelihood (Burda et al. 2015). The resulting IWAE bound, corresponding to the ELBO in Eq. (3), can be written as

$$\mathcal{L}_K^{IWAE}(\theta, \psi) = \mathbb{E}_{\mathbf{Z}_k \sim q_\theta(\mathbf{Z}|\mathbf{X})} \log \left[\frac{1}{K} \sum_{k=1}^K \frac{p_\psi(\mathbf{X}|\mathbf{Z}_k)p(\mathbf{Z}_k)}{q_\theta(\mathbf{Z}_k|\mathbf{X})} \right] \quad (5)$$

$$\hat{\mathcal{L}}_K^{IWAE}(\theta, \psi) = \log \left[\frac{1}{K} \sum_{k=1}^K \frac{p_\psi(\mathbf{X}|\tilde{\mathbf{Z}}_k)p(\tilde{\mathbf{Z}}_k)}{q_\theta(\tilde{\mathbf{Z}}_k|\mathbf{X})} \right]. \quad (6)$$

Importantly, although K samples are drawn from $q(\mathbf{Z}|\mathbf{X})$ to estimate the lower bound for both the VAE and IWAE, a VAE assumes a single latent variable \mathbf{Z} that is sampled K times, whereas an IWAE assumes $\mathbf{Z}_1, \dots, \mathbf{Z}_K$ are independent and identically distributed (i.i.d.) latent variables, and each variable is sampled once from $q(\mathbf{Z}|\mathbf{X})$. Typically, just one sample is drawn for each latent variable to estimate the ELBO and IWAE bound. If $K = 1$, $\mathcal{L}_1^{IWAE} = \mathcal{L}^{VAE}$, and the IWAE corresponds exactly to the standard VAE. For $K > 1$, Burda et al. (2015) showed that $\log p(\mathbf{X}) \geq \hat{\mathcal{L}}_{K+1}^{IWAE} \geq \hat{\mathcal{L}}_K^{IWAE}$, such that $\hat{\mathcal{L}}_K^{IWAE} \rightarrow \log p(\mathbf{X})$ as $K \rightarrow \infty$ if $p_\psi(\mathbf{X}, \mathbf{Z})/q_\theta(\mathbf{Z}|\mathbf{X})$ is bounded. Thus, the IWAE bound more closely approximates the true marginal log likelihood when $K > 1$ (Cremer et al. 2017), but the computational burden is increased due to the increased number of samples. A visualization of the workflow for an IWAE can be found in Appendix A3 of the supplementary materials.

2.4.3 dlglm: Modeling \mathbf{X} in the presence of missingness

Now, we extend the above framework to the deeply-learned GLM framework, where features within \mathbf{X} are partially observed during training. We formally introduce the *dlglm* model to handle MNAR missingness in the context of deeply-learned GLMs, as well as a

variant of *dlglm* to specifically handle MCAR and MAR missingness.

Let us define $q_\theta(\mathbf{Z}, \mathbf{X}^m)$ as the variational joint posterior pertaining to $(\mathbf{Z}, \mathbf{X}^m)$. We can factor this variational joint posterior as $q_\theta(\mathbf{Z}, \mathbf{X}^m) = q_{\theta_1}(\mathbf{Z}|\mathbf{X}^o)q_{\theta_2}(\mathbf{X}^m|\mathbf{Z}, \mathbf{X}^o, \mathbf{R})$. Here, for $k = 1, \dots, K$, we assume $\mathbf{Z}_k \stackrel{i.i.d.}{\sim} q_{\theta_1}(\mathbf{Z}|\mathbf{X}^o)$ similar to an IWAE, and additionally assume $\mathbf{X}_k^m \stackrel{i.i.d.}{\sim} q_{\theta_2}(\mathbf{X}^m|\mathbf{Z}, \mathbf{X}^o, \mathbf{R})$, where each \mathbf{X}_k^m has dimensionality p_{miss}^X . We utilize the class of factored variational posteriors, such that $q_\theta(\mathbf{Z}, \mathbf{X}^m) = \prod_{i=1}^n q_\theta(\mathbf{z}_i, \mathbf{x}_i^m)$ and $q_\theta(\mathbf{z}_i, \mathbf{x}_i^m) = q_{\theta_1}(\mathbf{z}_i|\mathbf{x}_i^o)q_{\theta_2}(\mathbf{x}_i^m|y_i, \mathbf{z}_i, \mathbf{x}_i^o, \mathbf{r}_i^X)$, with $\theta = \{\theta_1, \theta_2\}$. Then, denoting \mathbf{z}_{ik} and \mathbf{x}_{ik}^m as the i^{th} observation vectors of \mathbf{Z}_k and \mathbf{X}_k^m , respectively, we have $\mathbf{z}_{i1}, \dots, \mathbf{z}_{iK} \stackrel{i.i.d.}{\sim} q_{\theta_1}(\mathbf{z}_i|\mathbf{x}_i^o)$ and $\mathbf{x}_{i1}^m, \dots, \mathbf{x}_{iK}^m \stackrel{i.i.d.}{\sim} q_{\theta_2}(\mathbf{x}_i^m|y_i, \mathbf{z}_i, \mathbf{x}_i^o, \mathbf{r}_i^X)$. In this case, the lower bound, which we call the “*dlglm* bound”, can be derived as follows:

$$\begin{aligned} \log p_{\alpha, \beta, \pi, \psi, \phi}(\mathbf{X}^o, \mathbf{Y}, \mathbf{R}^X) &= \sum_{i=1}^n \log p_{\alpha, \beta, \pi, \psi, \phi}(\mathbf{x}_i^o, y_i, \mathbf{r}_i^X) \\ &= \sum_{i=1}^n \log \left[\iint p_{\alpha, \beta, \pi, \psi, \phi}(\mathbf{x}_i^o, \mathbf{x}_i^m, y_i, \mathbf{r}_i^X, \mathbf{z}_i) d\mathbf{z}_i d\mathbf{x}_i^m \right] \\ &= \sum_{i=1}^n \log \mathbb{E}_{(\mathbf{z}_{ik}, \mathbf{x}_{ik}^m) \sim q_\theta(\mathbf{z}_i, \mathbf{x}_i^m)} \left[\frac{1}{K} \sum_{k=1}^K \frac{p_{\alpha, \beta, \pi, \psi, \phi}(\mathbf{x}_i^o, \mathbf{x}_{ik}^m, y_i, \mathbf{r}_i^X, \mathbf{z}_{ik})}{q_\theta(\mathbf{z}_{ik}, \mathbf{x}_{ik}^m)} \right] \\ &\geq \sum_{i=1}^n \mathbb{E}_{(\mathbf{z}_{ik}, \mathbf{x}_{ik}^m) \sim q_\theta(\mathbf{z}_i, \mathbf{x}_i^m)} \log \left[\frac{1}{K} \sum_{k=1}^K \frac{p_{\alpha, \beta, \pi, \psi, \phi}(\mathbf{x}_i^o, \mathbf{x}_{ik}^m, y_i, \mathbf{r}_i^X, \mathbf{z}_{ik})}{q_\theta(\mathbf{z}_{ik}, \mathbf{x}_{ik}^m)} \right] = \mathcal{L}_K^{dlglm}, \quad (7) \end{aligned}$$

Here, $\{\psi, \beta, \pi, \phi, \theta\}$ are the weights and biases associated with the neural networks that output the parameters of the distributions that are involved, α is the dispersion parameter associated with the variance function of \mathbf{Y} , and $\tilde{\mathbf{z}}_{ik}$ and $\tilde{\mathbf{x}}_{ik}^m$ are the samples drawn from $q_{\theta_1}(\mathbf{z}_i|\mathbf{x}_i^o)$, and $q_{\theta_2}(\mathbf{x}_i^m|\mathbf{z}_i, \mathbf{x}_i^o, y_i, \mathbf{r}_i^X)$, respectively.

As discussed in Section 2.3, we use the selection model factorization of the complete data log-likelihood, such that $p_{\alpha, \beta, \pi, \psi, \phi}(\mathbf{x}_i^o, \mathbf{x}_i^m, y_i, \mathbf{r}_i^X, \mathbf{z}_i) = p_{\alpha, \beta, \pi}(y_i|\mathbf{x}_i)p_\psi(\mathbf{x}_i|\mathbf{z}_i)p(\mathbf{z}_i)p_\phi(\mathbf{r}_i^X|\mathbf{x}_i, y_i)$. Applying this factorization to (7), we obtain the form of the estimate of the “*dlglm* bound”, where the integral is estimated via Monte Carlo integration:

$$\hat{\mathcal{L}}_K^{dlglm} = \sum_{i=1}^n \log \left[\frac{1}{K} \sum_{k=1}^K \frac{p_{\alpha, \beta, \pi}(y_i|\mathbf{x}_i^o, \tilde{\mathbf{x}}_{ik}^m)p_\psi(\mathbf{x}_i|\tilde{\mathbf{z}}_{ik})p(\tilde{\mathbf{z}}_{ik})p_\phi(\mathbf{r}_i^X|y_i, \mathbf{x}_i^o, \tilde{\mathbf{x}}_{ik}^m)}{q_{\theta_1}(\tilde{\mathbf{z}}_{ik}|\mathbf{x}_i^o)q_{\theta_2}(\tilde{\mathbf{x}}_{ik}^m|\tilde{\mathbf{z}}_{ik}, \mathbf{x}_i^o, y_i, \mathbf{r}_i^X)} \right], \quad (8)$$

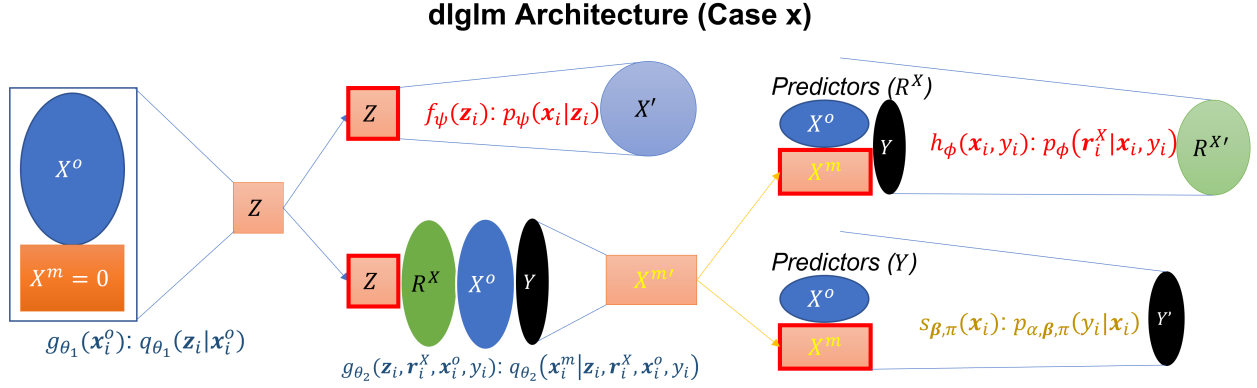


Figure 2: Architecture of proposed dlglm method (*Case x*). Dark colored nodes ($X^o, X^m = 0, R^X, Y$) represent deterministic values, lightly colored nodes (Z, X^o, X^m, R^X, Y') represent learned distributional parameters, and outlined (in red) nodes represent sampled values. Orange cells correspond to latent variables \mathbf{Z} and \mathbf{X}^m . $\mathbf{Z}_1, \dots, \mathbf{Z}_K$ and $\mathbf{X}_1^m, \dots, \mathbf{X}_K^m$ are sampled from their respective variational posteriors $q_{\theta_1}(\mathbf{Z}|\mathbf{X}^o)$ and $q_{\theta_2}(\mathbf{X}^m|\mathbf{Z}, \mathbf{R}^X, \mathbf{X}^o, \mathbf{Y})$.

We see that this quantity closely resembles the lower bound of an IWAE, and, similar to traditional VAEs, we utilize neural networks $f_{\psi}(\mathbf{z}_i)$, $g_{\theta_1}(\mathbf{x}_i^o)$, $g_{\theta_2}(\mathbf{z}_i, \mathbf{x}_i^o, \mathbf{r}_i^X, y_i)$, $s_{\beta, \pi}(\mathbf{x}_i)$, and $h_{\phi}(\mathbf{x}_i, y_i)$ to learn the values of the parameters of $p_{\psi}(\mathbf{x}_i|\mathbf{z}_i)$, $q_{\theta_1}(\mathbf{z}_i|\mathbf{x}_i^o)$, $q_{\theta_2}(\mathbf{x}_i^m|\mathbf{z}_i, \mathbf{x}_i^o, \mathbf{r}_i^X, y_i)$, $p_{\alpha, \beta, \pi}(y_i|\mathbf{x}_i)$, and $p_{\phi}(\mathbf{r}_i^X|\mathbf{x}_i, y_i)$. The associated weights and biases of the neural networks $\{\beta, \pi, \psi, \phi\}$, as well as the dispersion parameter α pertaining to $p_{\alpha, \beta, \pi}(\mathbf{Y}|\mathbf{X})$ are updated using stochastic gradient descent via the ADAM optimizer (Kingma & Ba 2014). The architecture of *dlglm* can be found in Figure 2. A pseudo-algorithm of *dlglm* can be found in Appendix A4 of the supplementary materials. We limited our discussion in this paper to *Case x*, where missingness exists only in \mathbf{X} but not in \mathbf{Y} ; however, the lower bound for *dlglm* can similarly be derived for the more general *Case xy* as well, and this derivation can be found in Appendix A5 of the supplementary materials.

We can obtain a variant of this method, which we call ignorably-missing dlglm (*idlglm*), by assuming independence between \mathbf{X}^m and \mathbf{R} by omitting \mathbf{r}_i^X from Equation 7, and removing $p_{\phi}(\mathbf{r}_i^X|y_i, \mathbf{x}_i^o, \tilde{\mathbf{x}}_{ik}^m)$ and letting $p_{\phi}(\tilde{\mathbf{x}}_{ik}^m|\tilde{\mathbf{z}}_{ik}, \mathbf{x}_i^o, y_i, \mathbf{r}_i^X) \rightarrow p_{\phi}(\tilde{\mathbf{x}}_{ik}^m|\tilde{\mathbf{z}}_{ik}, \mathbf{x}_i^o, y_i)$ in Equation 8. Whereas *dlglm* is better suited to handle MNAR, *idlglm* may be more appropriate for the MCAR or MAR settings, where a missingness model need not be specified.

In this paper, we are primarily interested in supervised learning. However, following training, *dlglm* and *idlglm* can also perform imputation as in the unsupervised learning

architecture for handling missingness proposed by Lim et al. (2021), although such imputation is not necessary for training, coefficient estimation, or prediction. The single imputation procedure, and additional computational details of *dlglm* and *idlgm* can be found in Appendix A6 and A1 of the supplementary materials, respectively.

3 Numerical Examples

In this section, we evaluate the performance of *dlglm* and *idlgm* to analyze each method’s performance in imputation, coefficient estimation, and prediction tasks on simulated datasets under MCAR, MAR, and MNAR missingness in Section 3.1. We also compare our methods to two commonly used approaches for modeling missing data in the supervised setting, mean imputation and the *mice* method for multiple imputation (Van Buuren & Groothuis-Oudshoorn 2011). To account for potential non-linearity and complex relationships between features, in Section 3.2, we mask completely-observed datasets obtained from the UCI Machine Learning Repository with varying mechanisms of missingness on the predictors. Finally, in Section 3.3, we perform prediction on the Bank Marketing dataset, which inherently contains missingness in the predictors.

3.1 Simulated Data

3.1.1 Simulation Setup

We first utilized completely synthetic data to evaluate the performance of each. Here, \mathbf{X} is generated such that $\mathbf{X} = \text{normalize}(\mathbf{Z}\mathbf{W} + \mathbf{B}) + B_0$, where *normalize*(\cdot) takes an input matrix and standardizes each column to mean 0 and standard deviation 1, and \mathbf{W} and \mathbf{B} are matrices of dimensions $d \times p$ and $n \times p$, respectively, $\mathbf{Z} \sim N_d(\mathbf{0}, \mathbf{I})$, and $W_{lj} \sim N(0, 0.5)$ and $B_{ij} \sim N(0, 1)$ for $i = 1, \dots, n$, $p = 1, \dots, p$, and $l = 1, \dots, d$, and $B_0 = 2$ is fixed. We also generated a binary response variable \mathbf{Y} such that $\Pr(\mathbf{Y} = 1|\mathbf{X}) = \beta_0 + \beta\mathbf{X}$, where β are drawn randomly from $\{-\frac{1}{4}, \frac{1}{4}\}$, and β_0 is chosen such that approximately half of the sample are in either class. Values of \mathbf{Y} are drawn from Bernoulli($\Pr(\mathbf{Y} = 1|\mathbf{X})$).

We then simulate the missingness mask matrix \mathbf{R}^X such that 50% of features in \mathbf{X} are partially observed, and 30% of the observations for each of these features are missing. We generate r_{ij} from the Bernoulli distribution with probability equal to $p(r_{ijm} = 1|\mathbf{x}_i, y_i, \phi)$,

such that $\text{logit}[p(r_{ij_m} = 1|\mathbf{x}_i, y_i, \boldsymbol{\phi})] = \phi_0 + \phi_1 y_i + \boldsymbol{\phi}_2 \mathbf{x}_i^o + \boldsymbol{\phi}_3 \mathbf{x}_i^m$, where $j_m = 1, \dots, p_{miss}^X$ index the missing features, ϕ_1 is the coefficient pertaining to the response, $\boldsymbol{\phi}_2 = \{\phi_{21}, \dots, \phi_{2, p_{obs}^X}\}$ are the coefficients pertaining to the observed features, and $\boldsymbol{\phi}_3 = \{\phi_{31}, \dots, \phi_{3, p_{miss}^X}\}$ are those pertaining to the missing features, where p_{obs}^X and p_{miss}^X are the total number of features that are observed and missing, respectively, with $p_{miss}^X = \text{floor}(0.5 * p)$ and $p_{obs}^X = p - p_{miss}^X$. Here, we fixed $\phi_1 = 0$, and drew nonzero values of $\{\boldsymbol{\phi}_2, \boldsymbol{\phi}_3\}$ from the log-normal distribution with mean $\mu_\phi = 5$, with log standard deviation $\sigma_\phi = 0.2$.

To evaluate the impact of the misspecification of the missingness mechanism on model performance, r_{ij_m} was simulated under each mechanism as follows: (1) MCAR: $\{\phi_1, \boldsymbol{\phi}_2, \boldsymbol{\phi}_3\} = 0$ (2) MAR: Same as MCAR except $\phi_{2j_o} \neq 0$ for one completely-observed feature j_o (3) MNAR: Same as MCAR except $\phi_{3j_m} \neq 0$ for one missing feature j_m . In this way, for each MAR or MNAR feature, the missingness is dependent on just one feature. In each case, we used ϕ_0 to control for an expected rate of missingness of 30% in each partially-observed feature. We note that for each these simulations, we utilize all features in \mathbf{X} as well as the response \mathbf{Y} as input into *dlglm*'s missingness network, although only one feature is involved under the true missingness model.

We vary n and d such that $n = \{10,000, 100,000\}$ and $d = \{2, 8\}$, and fix $p = 50$. We simulated 5 datasets per simulation condition, spanning various missingness mechanisms and values for $\{n, d\}$. We fix the values of $\boldsymbol{\beta}$ at 0.25 for each feature, and adjusted β_0 to ensure equal proportions for the binary class response \mathbf{Y} . For each simulation case, we partitioned the data into training, validation, and test sets with ratio 8:1:1. For *mice* imputation, we averaged across 500 multiply-imputed datasets to obtain a single imputed dataset. We note that we generated \mathbf{Y} by a linear transformation of \mathbf{X} in these simulations in order to facilitate fair comparisons with *mice*, which cannot account for non-linear relationships between the features and the response. Because no hyperparameter tuning is required, the validation set is not utilized for *mice* and mean imputation.

We measured the performance of each method with respect to three different tasks: imputation of missing values, coefficient estimation, and prediction. Imputation performance was measured with respect to the truth on a single imputed dataset by mean, *dlglm* and

idlglm imputation, and on an average of multiply-imputed datasets by *mice*. Coefficient estimation for mean and *mice* were based on downstream fitted GLM(s) on these imputed dataset(s), where estimates were pooled using Rubin’s rules (Rubin 2004) for *mice*. For *dlglm* and *idlglm*, we estimated the coefficients by the weights and bias β of the last layer of the $s_{\beta,\pi}(\cdot)$ trained neural network. Here, we fixed the number of hidden layers in $s_{\beta,\pi}(\cdot)$ to 0 to allow for direct comparison with the other methods. A more complex prediction model via a neural network can be learned by simply incorporating additional hidden layers in $s_{\beta,\pi}(\cdot)$. We note that *dlglm* and *idlglm* can estimate β without having to perform multiple imputation and downstream modelling like *mice*, where fitting complex methods such as neural networks each of the multiply-imputed datasets separately may be computationally prohibitive.

After obtaining the coefficient estimates and trained models, we performed prediction on the test set in two ways: 1) using the incomplete (predI) test set, where the true values of \mathbf{X}^m are not known at prediction time, and 2) using the complete (predC) test set, where the true simulated values of \mathbf{X}^m are known at prediction time. These two ways reflect the two realistic cases in which (1) missingness is present during training time but complete data is available at prediction time, and (2) missingness is present during both training and prediction time. For predI, *mice* and mean imputation require an additional imputation step on the test set before predicting \mathbf{Y} ; for *dlglm* and *idlglm*, we simply input the incomplete test set into the trained model without needing to separately impute the test set, and we predict using the trained model. That is, *mice* and mean imputation cannot generalize the trained model to impute the test set, *dlglm* and *idlglm* provide a seamless framework to utilize the already-trained model to impute and predict on a held-out test set. For predC, we use the underlying true values of \mathbf{X}^m to predict on the test dataset.

Imputation error was measured by the average L1 distance between true and imputed masked values in \mathbf{X} . Letting $\hat{\mathbf{X}}^m$ denote the imputed masked values of the true \mathbf{X}^m values of the missing entries, we denote the average L1 distance is simply $\frac{|\hat{\mathbf{X}}^m - \mathbf{X}^m|}{N_{miss}}$, where N_{miss} is the total number of missing entries in the dataset. Performance in coefficient estimation was measured by the average percent bias (PB) of the coefficient estimates compared to

the truth, averaged across the p features, i.e. $PB = \frac{1}{p} \sum_{j=1}^p \frac{|\beta_j - \hat{\beta}_j|}{|\beta_j|}$. Finally, predC and predI prediction error was measured by the average L1 distance between predicted and true values of the probabilities of class membership $\Pr(\mathbf{Y} = 1|\mathbf{X})$ in the test set.

3.1.2 Simulation Results

Figures 3 and 4 illustrate the simulation results pertaining to imputation accuracy, coefficient estimation, and prediction accuracy for the condition $p = 50$. We see that across all combinations of $\{n, d\}$ and mechanisms of missingness, mean imputation consistently performs poorly in imputation, coefficient estimation, and prediction, while *mice* and *idlglm* perform comparably in these metrics. Also, we note that under MNAR missingness, *dlglm* generally yields the lowest imputation and prediction error, as well as percent bias across all simulation cases. Under MAR missingness, *dlglm* performs comparably to *idlglm* and *mice*. This shows the ability of *dlglm* to learn an accurate model of the missingness, even under severe overparametrization of the missingness model (model need not be specified for ignorable missingness). However, due to the complexity of the model, we see that *dlglm* does generally perform poorly compared to *idlglm* and *mice* under MCAR missingness, when $n = 10,000$, although it still performs comparably to other methods when the sample size is very large ($n = 100,000$). As one may expect, prediction performance using the incomplete data (predI) was poorer than prediction performance using the complete data (predC) for all methods.

We additionally show results pertaining to $p = 25$ in Appendix B2 of the supplementary materials. We similarly found that *dlglm* performed best under MNAR missingness, and comparably to *idlglm* and *mice* under MCAR and MAR missingness.

3.2 Real Data with Simulated Missingness

Next, we analyzed 3 completely-observed, large datasets from the UCI Machine Learning Repository (Dua & Graff 2017) that contained a specific response variable of interest, in order to preserve non-linearity and interactions between observed features. The DRY-BEAN dataset contains 16 features describing 13,611 images of dry beans taken with a high-resolution camera, and the response variable of interest was the type of dry bean each image represents, with 7 different possible types of beans. The LETTER dataset contains

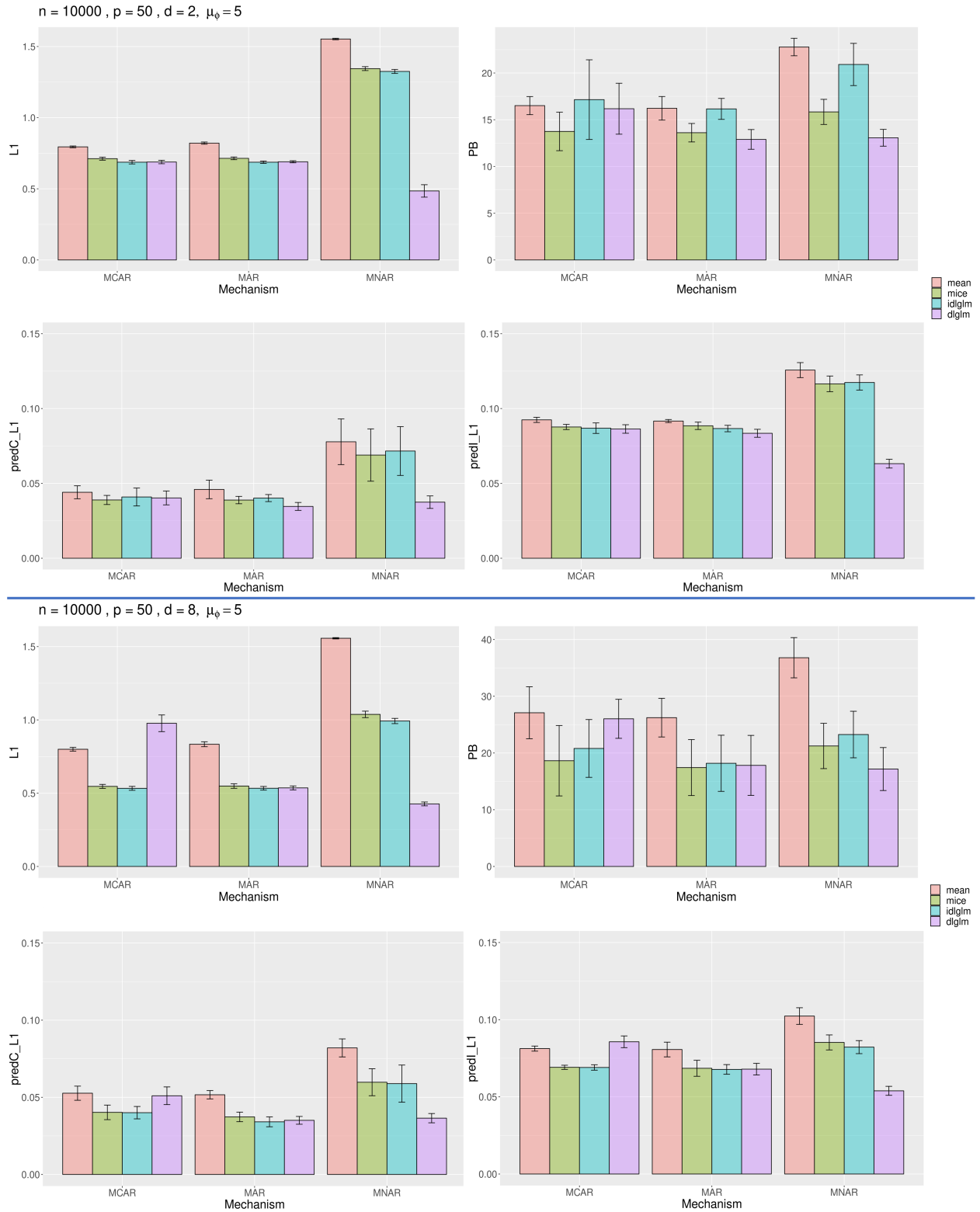


Figure 3: Simulation results with $n = 10,000$ and $p = 50$, varying $d = 2$ (top 4) and $d = 8$ (bottom 4). In each quadrant, we measure imputation accuracy by the average L1 distance between imputed vs true values in \mathbf{X} (top-left), coefficient estimation accuracy by the average percent bias (PB) of the estimates $\hat{\beta}$ compared to the truth (top-right), and prediction accuracy by the average L1 distance between the predicted and true probabilities of class 1 membership of \mathbf{Y} using the true unmasked test set (predC, bottom-left) and the incomplete test set (predI, bottom-right). In predI, we first impute missing values of the test data for mean and *mice* imputation, and we input the incomplete test set as-is for *dglm* and *idglm*.

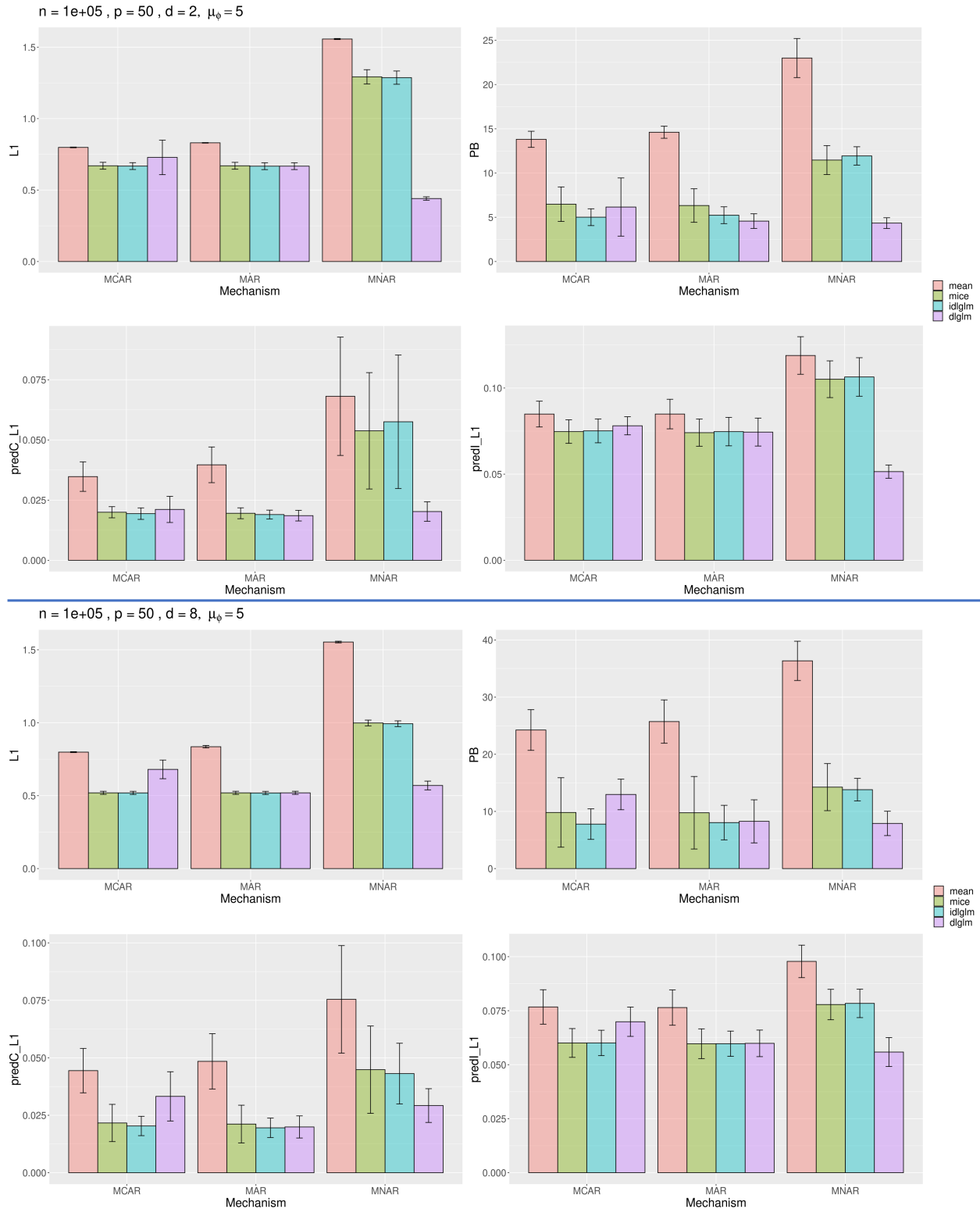


Figure 4: Simulation results with $n = 100,000$ and $p = 50$, varying $d = 2$ (top 4) and $d = 8$ (bottom 4). In each quadrant, we measure imputation accuracy by the average L1 distance between imputed vs true values in \mathbf{X} (top-left), coefficient estimation accuracy by the average percent bias (PB) of the estimates $\hat{\beta}$ compared to the truth (top-right), and prediction accuracy by the average L1 distance between the predicted and true probabilities of class 1 membership of \mathbf{Y} using the true unmasked test set (predC, bottom-left) and the incomplete test set (predI, bottom-right). In predI, we first impute missing values of the test data for mean and *mice* imputation, and we input the incomplete test set as is for *dlglm* and *idlgm*.

16 attributes of 20,000 black-and-white pixel images, each displaying one English letter (A to Z). Finally, the SHUTTLE dataset contains 9 numerical attributes pertaining to 58,000 shuttle stat logs (observations), which are classified into 7 different categories. Due to a low sample size in 4 of the 7 categories, we pre-filtered the observations pertaining to these categories out of the dataset, and the resulting dataset contained 57,756 observations of 3 categories. In each of these datasets, the response variable was multi-category. Additional information regarding these datasets, and how to obtain the raw data files can be found in Appendix C of the supplementary materials.

We then simulated the missingness mask \mathbf{R}^X with MCAR, MAR, and MNAR patterns of missingness in the manner described in Section 3.1.1. We split the samples in each dataset by a similar 8:1:1 ratio of training/validation/test samples. In the test set samples, we then imputed the missing values and predicted the response variables with each method in a manner similar to Section 3.1.1. For *dlglm* and *idlglm*, We account for potential nonlinear relationships between the covariates and response by allowing the number of hidden layers in $s_{\beta,\pi}(\cdot)$ to be nonzero in hyperparameter tuning. Then, we compared imputation and prediction accuracy on each dataset, under each mechanism of missingness. Since the underlying true probabilities of class membership were unavailable, we measured prediction accuracy by the Cohen’s kappa metric on the complete (kappaC) and incomplete (kappaI) test set. This metric measures how accurately a binary class variable was predicted, with a value of -1 indicating worst possible performance, and a value of 1 indicating perfect concordance with the truth.

Results from the imputation and prediction analyses on these datasets can be found in Figure 5. We found that, as in the simulations, mean imputation performed most poorly in both imputation and downstream prediction, while *dlglm* tended to perform best in the MNAR cases, and performed comparably to *mice* and *idlglm* under the MCAR and MAR cases. This further validates our claims under a more realistic setting, where the true data generation mechanism may be unknown. We also see that under both MCAR and MAR missingness, *mice* performed worse than *idlglm* in prediction on the LETTER and SHUTTLE datasets. This is particularly interesting since *mice* is a widely-used algorithm

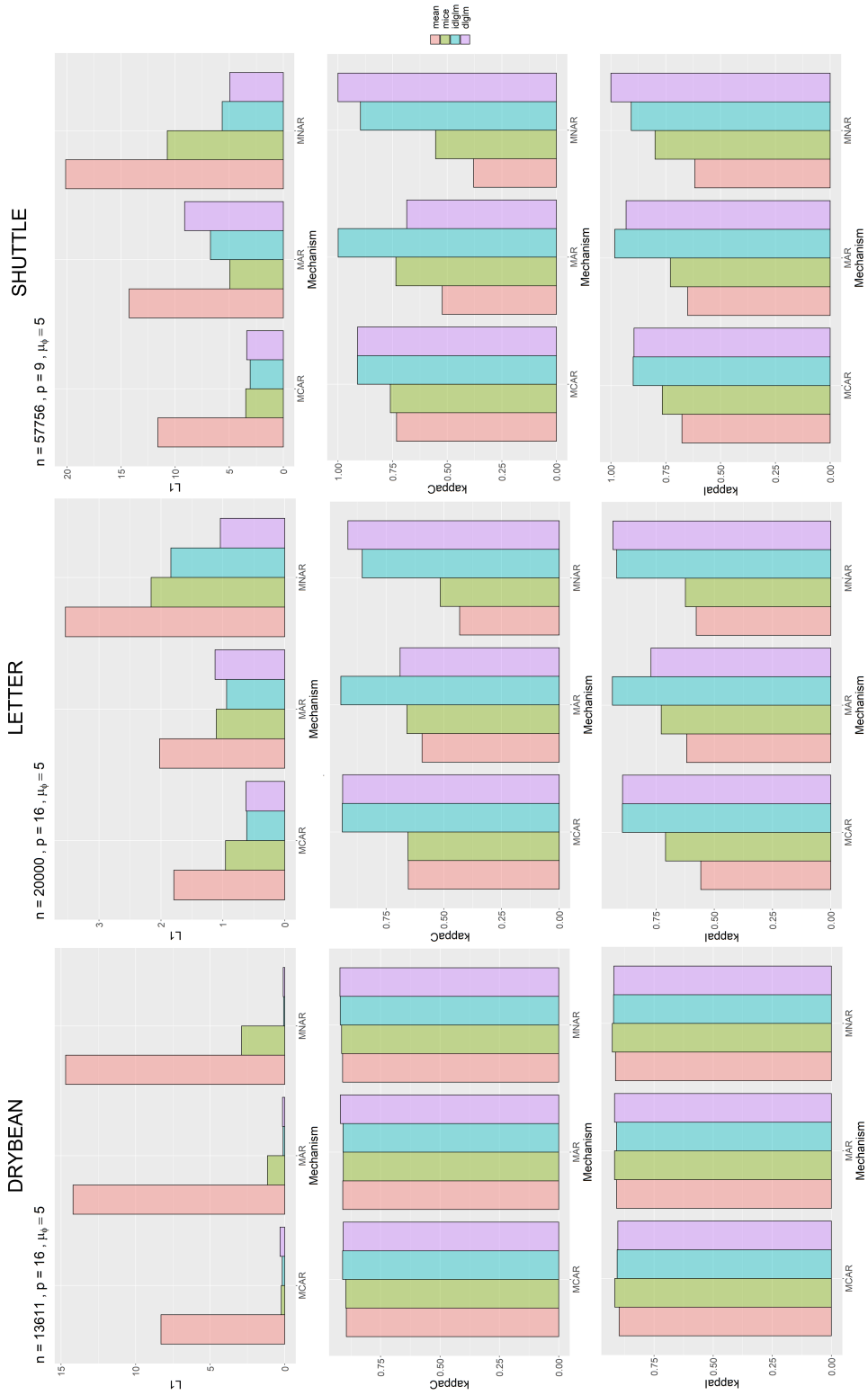


Figure 5: Imputation (top row) and prediction results from predC (middle row) and predI (bottom row) from comparative methods run on 3 large datasets from the UCI Machine Learning Repository: DRYBEAN, LETTER, and SHUTTLE (columns, left to right). Imputation error was measured by the average L1 distance between true and imputed entries, with lower values indicating better performance, and prediction performance was measured by the Cohen's kappa metric for both predC (kappaC) and predI (kappaI), with higher values indicating better performance.

that has been shown to perform well under ignorable missingness (Van Buuren & Groothuis-Oudshoorn 2011). However, the *mice* model has been known to break down under nonlinear relationships between the features (Van Buuren 2018), as may be the case in many real-world datasets like these. Using neural networks to model the data generation process allows *idlgm* to better model potential nonlinear relationships between features, allowing for more accurate prediction.

Interestingly, all of the algorithms performed similarly in prediction on the DRYBEAN dataset. However, we found that this dataset contained extremely high levels of correlation between the variables (see Web Appendix C of the supplementary materials). Highly-correlated features may cause some missing features to be redundant in the prediction model, thus reducing the importance of an accurate method to properly account for the missingness. Intuitively, when features containing missingness are highly correlated to other fully-observed features, such missingness may not truly reflect the MNAR scenario (Hapfelmeier et al. 2012). This is because there exist fully-observed features that are highly correlated with the missing features, and ignorably-missing data methods like *idlgm* may gather information about the missing entries from these correlated, fully-observed features without having to explicitly model the mechanism of missingness. Still, *idlgm* and *dlglm* imputed missing entries much more accurately than *mean* and *mice* under MAR and MNAR. Interestingly, we also see that *idlgm* performed similarly to *dlglm* under MNAR in this dataset.

We additionally performed similar analyses on 5 other smaller UCI datasets, and these results can be found in Appendix D of the supplementary materials. We found that under small sample size settings, performance via *dlglm* was more variable under MNAR. We suggest use of *dlglm* when the data contains at least 10,000 samples, as the model may be too complex to be accurately trained under smaller sample sizes.

3.3 Bank Marketing Dataset

Finally, we performed prediction on the Bank Marketing dataset from the UCI Machine Learning Repository. This dataset contained 41,188 observations of 20 different attributes that were obtained based on direct phone calls from a Portuguese banking institution as

part of a promotion campaign for a term deposit subscription (Moro et al. 2014). The response variable of interest was a fully-observed binary measure of whether the client subscribed a term deposit. Of the 20 attributes, we removed 1 attribute as directed from the manual due to perfect correlation with the response variable, and removed 3 other attributes that were deemed irrelevant to the prediction task: month of contact, day of contact, and communication type (cell phone or telephone).

Missingness was present in 8 of the 16 attributes: type of job, marital status, level of education, whether the client had a credit in default, whether the client had a housing loan, whether the client had a personal loan, number of days since the client was contacted in a previous campaign, and outcome of the previous campaign. The remaining 8 attributes were fully-observed: age of client, number of contacts during this campaign, number of contacts before this campaign, employment variation rate, consumer price index, consumer confidence index, euribor 3 month rate, and employee number. The global rate of missingness was about 13.3%. The response variable of interest was collected by additional follow-up calls to confirm whether the client subscribed to the product. Additional information regarding the bank marketing dataset, and how to obtain the raw data files can be found in Appendix E of the supplementary materials.

This type of dataset reflects the most realistic situation in practice, where missingness exists in a dataset and one has no prior knowledge of either the relationships between the features and the response, or the underlying mechanism of the missingness. We divided the dataset into the 8:1:1 training, validation, and test set ratio, and performed prediction as before. Because neither the data nor the missingness was simulated, we compared just the predI prediction performance across the methods.

Table 1 shows the results from these prediction analyses. We measured prediction performance of the binary response variable by 4 metrics: Area Under the ROC Curve (AUC), Positive Predictivity (PPV), Cohen’s kappa (κ), and the F1 metric. For each metric, a larger value represents greater concordance between the true and predicted response. We see that *dlglm* yielded a significantly greater performance in prediction via all metrics, which suggests that the missingness present in this dataset may be MNAR, as *dlglm* is the

	AUC	PPV	kappa	F1
dlglm	0.88	0.481	0.445	0.516
idlglm	0.779	0.446	0.411	0.488
mean	0.769	0.448	0.385	0.46
mice	0.771	0.455	0.396	0.471

Table 1: Results from prediction analyses on the Bank Marketing dataset from the UCI Machine Learning Repository. We measured concordance between the true and predicted binary response by 4 metrics: Area Under ROC Curve (AUC), Positive Predictivity (PPV), Cohen’s kappa (kappa), and F1 score.

only method that accounts for MNAR missingness. This is in line with previous studies on missingness in survey data, which researchers have oftentimes considered MNAR (de Leeuw 2001)

Also, we note that predictions via *idlglm* yielded slightly greater AUC, F1, and Cohen’s kappa than *mice* imputation, but slightly lower PPV. This is reflective of the properties seen in the simulations, where *idlglm* performed comparably to *mice* in each simulated mechanism of missingness. Since these are both methods catered to handle ignorably-missing data, they would likely yield biased models under MNAR missingness, as may be the case in this dataset. Additionally, we see that *mice* and mean imputation yielded similar performance via all metrics. This may be due to the fact that these methods are impute-then-regress methods, unlike *dlglm* and *idlglm*, and thus downstream prediction performance may be less affected by the method of imputation employed (Le Morvan et al. 2021).

4 Discussion

In this paper, we introduced a novel deep learning method called Deeply-learned Generalized Linear Model with Missing Data (*dlglm*), which is able to perform coefficient estimation and prediction in the presence of missing not at random (MNAR) data. *dlglm* utilizes a deep learning neural network architecture to model the generation of the data

matrix \mathbf{X} , as well as the relationships between the response variable \mathbf{Y} and \mathbf{X} and between the missingness mask \mathbf{R} and \mathbf{X} . In this way, we are able to (1) generalize the traditional GLM to account for complex nonlinear interactions between the features, and (2) account for ignorable and non-ignorable forms of missingness in the data. We also showed through simulations and real data analyses that *dlglm* performs better in coefficient estimation and prediction in the presence of MNAR missingness than other impute-then-regress methods, like mean and mice imputation. Furthermore, we found that *dlglm* was generally robust to the mechanism of missingness, performing comparably well to *mice* and *idlglm* under MCAR and MAR settings. Still, it is recommended to utilize *idlglm* when the missingness is ignorable, as the missingness model that is learned in *dlglm* is not necessary in the ignorable missingness setting.

A supervised learning algorithms such as *dlglm* and *idlglm* can be particularly useful in analyzing real-life data in the presence of missingness. In reality, the mechanism underlying missing values cannot be known or tested, however a flexible algorithm like *dlglm* that can be relatively robust to severe overparameterization of the missingness model can be pivotal to unbiased results. Furthermore, whereas impute-then-regress methods may typically require fully-observed observations at test time for prediction, *dlglm* and *idlglm* can predict the response of interest using partially-observed observations. This provides a convenient workflow, where a user need not separately re-impute the prediction set at test time.

In this paper, we focused specifically on the case of univariate response \mathbf{Y} . *dlglm* and *idlglm* can be generalized to the multivariate \mathbf{Y} case by (1) including \mathbf{Y} in the existing IWAE structure and (2) expanding the neural network $s_{\beta,\pi}(\mathbf{x}_i)$ to account for all q responses in \mathbf{Y} , and utilizing samples of \mathbf{Z} as additional input into this network such that $s_{\beta,\pi}(\mathbf{x}_i) \rightarrow s_{\beta,\pi}(\mathbf{x}_i, \mathbf{z}_i)$. By doing this, we account for multivariate \mathbf{Y} , outputting additional parameters pertaining to the newly-specified distribution of $p_{\beta,\pi}(\mathbf{y}_i|\mathbf{x}_i, \mathbf{z}_i)$ and modelling correlation of \mathbf{Y} by the learned latent structure. We leave this as an extension of our method.

SUPPLEMENTARY MATERIAL

Supplementary Materials: Additional details of the *dlglm* algorithm and the datasets used in this paper. (pdf)

R-package for dlglm: R-package *dlglm* containing code to perform the diagnostic methods described in the article. The package can be downloaded from <https://github.com/DavidKLim/dlglm> (website)

R Paper repo for reproducibility: Github repository to replicate all analyses from this paper can be found here: https://github.com/DavidKLim/dlglm_Paper (website)

References

Bottou, L. (2012), Stochastic gradient descent tricks, *in* ‘Neural networks: Tricks of the trade’, Springer, pp. 421–436.

Burda, Y., Grosse, R. & Salakhutdinov, R. (2015), ‘Importance Weighted Autoencoders’, *arXiv e-prints* p. arXiv:1509.00519.

Chen, D., Liu, S., Kingsbury, P., Sohn, S., Storlie, C. B., Habermann, E. B., Naessens, J. M., Larson, D. W. & Liu, H. (2019), ‘Deep learning and alternative learning strategies for retrospective real-world clinical data’, *npj Digital Medicine* **2**(1).

Cremer, C., Morris, Q. & Duvenaud, D. (2017), ‘Reinterpreting Importance-Weighted Autoencoders’, *arXiv e-prints* p. arXiv:1704.02916.

de Leeuw, E. D. (2001), ‘Reducing missing data in surveys: An overview of methods’, *Quality and Quantity* **35**(2), 147–160.

Diggle, P. & Kenward, M. G. (1994), ‘Informative drop-out in longitudinal data analysis’, *Applied Statistics* **43**(1), 49.

Dormehl, L. (2019), ‘What is an artificial neural network? here’s everything you need to know’.

URL: <https://www.digitaltrends.com/cool-tech/what-is-an-artificial-neural-network/>

Dua, D. & Graff, C. (2017), ‘UCI machine learning repository’.

URL: <http://archive.ics.uci.edu/ml>

- Friedman, J., Hastie, T. & Tibshirani, R. (2010), ‘Regularization paths for generalized linear models via coordinate descent’, *Journal of Statistical Software* **33**(1).
- Gershman, S. J. & Goodman, N. D. (2014), Amortized inference in probabilistic reasoning, *in* ‘CogSci’.
- Ghorbani, A. & Zou, J. Y. (2018), Embedding for informative missingness: Deep learning with incomplete data, *in* ‘2018 56th Annual Allerton Conference on Communication, Control, and Computing (Allerton)’, IEEE, pp. 437–445.
- Guo, H. & Gelfand, S. B. (1990), Analysis of gradient descent learning algorithms for multilayer feedforward neural networks, *in* ‘29th IEEE Conference on Decision and Control’, IEEE, pp. 1751–1756.
- Hapfelmeier, A., Hothorn, T., Ulm, K. & Strobl, C. (2012), ‘A new variable importance measure for random forests with missing data’, *Statistics and Computing* **24**(1), 21–34.
- Holland, P. W. & Welsch, R. E. (1977), ‘Robust regression using iteratively reweighted least-squares’, *Communications in Statistics - Theory and Methods* **6**(9), 813–827.
- Hoogland, J., Barreveld, M., Debray, T. P. A., Reitsma, J. B., Verstraelen, T. E., Dijkgraaf, M. G. W. & Zwinderman, A. H. (2020), ‘Handling missing predictor values when validating and applying a prediction model to new patients’, *Statistics in Medicine* **39**(25), 3591–3607.
- Ibrahim, J. G., Chen, M.-H., Lipsitz, S. R. & Herring, A. H. (2005), ‘Missing-data methods for generalized linear models’, *Journal of the American Statistical Association* **100**(469), 332–346.
- Ibrahim, J. G. & Molenberghs, G. (2009), ‘Missing data methods in longitudinal studies: a review’, *TEST* **18**(1), 1–43.
- Ipsen, N. B., Mattei, P.-A. & Frellsen, J. (2021), How to deal with missing data in supervised deep learning?, *in* ‘International Conference on Learning Representations’.

- Kingma, D. P. & Ba, J. (2014), ‘Adam: A Method for Stochastic Optimization’, *arXiv e-prints* p. arXiv:1412.6980.
- Kingma, D. P. & Welling, M. (2013), ‘Auto-Encoding Variational Bayes’, *arXiv e-prints* p. arXiv:1312.6114.
- Kingma, D. P. & Welling, M. (2019), ‘An Introduction to Variational Autoencoders’, *arXiv e-prints* p. arXiv:1906.02691.
- Le Morvan, M., Josse, J., Scornet, E. & Varoquaux, G. (2021), ‘What’s a good imputation to predict with missing values?’, *Advances in Neural Information Processing Systems* **34**.
- Lim, D. K., Rashid, N. U., Oliva, J. B. & Ibrahim, J. G. (2021), ‘Handling Non-ignorably Missing Features in Electronic Health Records Data Using Importance-Weighted Autoencoders’, *arXiv e-prints* p. arXiv:2101.07357.
- Lipsitz, S. R. & Ibrahim, J. G. (1996), ‘A conditional model for incomplete covariates in parametric regression models’, *Biometrika* **83**(4), 916–922.
- Little, R. J. A. & Rubin, D. B. (2002), *Statistical Analysis with Missing Data*, John Wiley & Sons, Inc.
- Lopez, R., Regier, J., Cole, M. B., Jordan, M. I. & Yosef, N. (2018), ‘Deep generative modeling for single-cell transcriptomics’, *Nature Methods* **15**(12), 1053–1058.
- McCullagh, P. & Nelder, J. A. (2019), *Generalized linear models*, Routledge.
- Moro, S., Cortez, P. & Rita, P. (2014), ‘A data-driven approach to predict the success of bank telemarketing’, *Decision Support Systems* **62**, 22–31.
- Murphy, J. (2016), ‘An overview of convolutional neural network architectures for deep learning’, *Microway Inc* pp. 1–22.
- Nelder, J. A. & Wedderburn, R. W. M. (1972), ‘Generalized linear models’, *Journal of the Royal Statistical Society. Series A (General)* **135**(3), 370–384.

- Prechelt, L. (1998), Early stopping-but when?, *in* ‘Neural Networks: Tricks of the trade’, Springer, pp. 55–69.
- Qi, M. & Wu, Y. (2003), ‘Nonlinear prediction of exchange rates with monetary fundamentals’, *Journal of Empirical Finance* **10**(5), 623–640.
- Razzak, M. I., Naz, S. & Zaib, A. (2017), Deep learning for medical image processing: Overview, challenges and the future, *in* ‘Lecture Notes in Computational Vision and Biomechanics’, Springer International Publishing, pp. 323–350.
- Rubin, D. B. (1976), ‘Inference and missing data’, *Biometrika* **63**(3), 581–592.
- Rubin, D. B. (2004), *Multiple imputation for nonresponse in surveys*, Vol. 81, John Wiley & Sons.
- Saxe, A. M., McClelland, J. L. & Ganguli, S. (2014), Exact solutions to the nonlinear dynamics of learning in deep linear neural network, *in* ‘In International Conference on Learning Representations’.
- Stubbenick, A. L. & Ibrahim, J. G. (2003), ‘Maximum likelihood methods for nonignorable missing responses and covariates in random effects models’, *Biometrics* **59**(4), 1140–1150.
- Svozil, D., Kvasnicka, V. & Pospichal, J. (1997), ‘Introduction to multi-layer feed-forward neural networks’, *Chemometrics and intelligent laboratory systems* **39**(1), 43–62.
- Tran, M.-N., Nguyen, N., Nott, D. & Kohn, R. (2019), ‘Bayesian deep net GLM and GLMM’, *Journal of Computational and Graphical Statistics* **29**(1), 97–113.
- Van Buuren, S. (2018), *Flexible imputation of missing data*, CRC press.
- Van Buuren, S. & Groothuis-Oudshoorn, K. (2011), ‘mice: Multivariate imputation by chained equations in r’, *Journal of statistical software* **45**(1), 1–67.
- Wells, B. J., Nowacki, A. S., Chagin, K. & Kattan, M. W. (2013), ‘Strategies for handling missing data in electronic health record derived data’, *eGEMs (Generating Evidence & Methods to improve patient outcomes)* **1**(3), 7.

Supporting Information for Deeply-Learned Generalized Linear Models with Missing Data

David K. Lim^{1,*},
Naim U. Rashid^{1,**},
Junier B. Oliva^{2,***}, and
Joseph G. Ibrahim^{1,****}

¹Department of Biostatistics, University of North Carolina at Chapel Hill,
Chapel Hill, NC, USA

²Department of Computer Science, University of North Carolina at Chapel
Hill, Chapel Hill, NC, USA

July 20, 2022

Appendix A: Additional Details

A1: Computational Details

In this section, we go through details of some of the computational methods involved in *dlglm* and *idlglm*.

Stochastic Gradient Descent

In most deep learning architectures, stochastic gradient descent (SGD) is the favored algorithm of optimization, as it is very scalable to higher dimensions. A typical SGD algorithm proceeds as follows: let Q be an objective function to be maximized and let Ω denote the collection of all parameters one wishes to maximize over. Also let $Q^{(t)}$ denote the value of

the objective function and $\hat{\Omega}^{(t)}$ denoting the estimate of Ω at update step t . Then, one can optimize Ω with respect to Q by some update rule $\hat{\Omega}^{(t+1)} = \hat{\Omega}^{(t)} + \delta \nabla_{\Omega} Q^{(t)}$, where δ is the step size which controls how large of a change is applied to the update, and the gradient ∇ is taken with respect to each parameter in Ω . In this way, Ω is updated at each step t such that $Q^{(t)}$ is increased, and the magnitude of the change in $\hat{\Omega}^{(t)}$ is mediated by δ .

There are many variants of SGD, including ADAM (Kingma & Ba 2014), ADMM (Boyd et al. 2011), Adagrad (Lydia & Francis 2019), and more, as well as a natural gradient variational approximation with factor covariance method as discussed by Tran et al. (2019). In *dlglm* and *idlglm*, we utilize ADAM as the default optimizer.

Reparameterization Trick

In a VAE, one uses the so-called reparameterization trick in order to draw samples from any continuous distribution $q_{\theta}(\mathbf{Z}|\mathbf{X})$ while allowing for a Monte Carlo estimate of the expectation in the lower bound to be differentiable with respect to θ (Kingma & Welling 2013). This is accomplished by expressing the random variable $\mathbf{Z} = g_{\theta}(\epsilon, \mathbf{X})$, where ϵ is an auxiliary variable with marginal distribution $p(\epsilon)$ and $g_{\theta}(\cdot)$ is some function with parameters θ . In a traditional VAE setting where $q_{\theta}(\mathbf{Z}|\mathbf{X})$ is a multivariate normal distribution with diagonal covariance structure, $\epsilon \sim N(0, 1)$, and $g_{\theta}(\epsilon, \mathbf{X}) = \boldsymbol{\mu}_Z + \boldsymbol{\sigma}_Z \cdot \epsilon$, where $\boldsymbol{\mu}_Z$ is the vector of means of $q_{\theta}(\mathbf{Z}|\mathbf{X})$, and $\boldsymbol{\sigma}_Z$ is the corresponding entries of the standard deviations from the diagonal covariance of $q_{\theta}(\mathbf{Z}|\mathbf{X})$.

In *dlglm* and *idlglm*, we multiply use the reparameterization trick for each of the K latent variable pairs $\{\mathbf{Z}_k, \mathbf{X}_k^m\}$. The standard reparameterization trick can be used when all of the covariates are continuous, such that a multivariate normal distributional assumption with

diagonal covariance structure may hold for both $q_{\theta_1}(\mathbf{z}_i|\mathbf{x}_i^o)$ and $q_{\theta_2}(\mathbf{x}_i^m|\mathbf{z}_i, \mathbf{x}_i^o, \mathbf{r}_i^X, y_i)$.

If some partially-observed covariates are categorical features, one can approximate a discrete categorical distribution with the Gumbel-Softmax distribution (Jang et al. 2016). In particular, without loss of generality, let \mathbf{X}^* be a vector of length n matrix consisting of one categorical feature in \mathbf{X} with C distinct classes, with entries x_1^*, \dots, x_n^* . Denote $\{x_{i1}^*, \dots, x_{iC}^*\}$ as the softmax probabilities of the categorical value of x_i^* for each class. Then, the density of the Gumbel-Softmax distribution is written as

$$p_{\rho, \tau}(x_{i1}^*, \dots, x_{iC}^*) = \Gamma(C)\tau^{C-1}(\sum_{c=1}^C \pi_c / (x_{ic}^*)^\tau)^{-C} \prod_{c=1}^C (\pi_c / (x_{ic}^*)^{\tau+1}),$$

where τ is the softmax temperature and ρ is the C class probabilities of x_i^* . Since this is a continuous distribution, samples can be drawn using the standard reparameterization trick. When $\tau \gg 0$, $\{x_{i1}^*, \dots, x_{iC}^*\}$ represent softmax samples that whose values are close to $1/C$. As $\tau \rightarrow 0$, samples drawn from $p_{\rho, \tau}(x_{i1}^*, \dots, x_{iC}^*)$ become one-hot, and this Gumbel-Softmax distribution becomes exactly the discrete categorical distribution.

Initialization

Initialization of weights and biases in deep learning architectures are typically done by drawing values centered around 0, such that the magnitudes of these parameters start off small, and those pertaining to important connections are increase in magnitude as training progresses, while the weights of unimportant connections tend towards 0. *dlglm* and *idlglm* uses the semi-orthogonal matrix initialization (Saxe et al. 2014) for π , β ψ , θ , and ϕ , where for each layer, a QR decomposition is performed on random values drawn from $N(0, 1)$ in order

to obtain an orthogonal matrix, whose entries are used as initialized values for the weights and bias pertaining to that layer. This procedure is repeated for each layer of each neural network.

An orthogonal matrix of initialized values for the weights and biases have the nice property of being norm-preserving, which has been shown to aid in deep neural networks to prevent exploding or vanishing signals during training (Saxe et al. 2014).

Early Stop Criterion

In *dlglm* and *idlglm*, we incorporate an early stop criterion (Prechelt 1998) in order to prevent overfitting on the training set, and to reduce computation time. Specifically, let $L^{(t)} \equiv \hat{\mathcal{L}}_{K,valid}^{dlglm,(t)}$ denote the estimated *dlglm* bound on a held-out validation set at each update step (t), and initialize $L_{opt} = L^{(0)}$ and $E^{(0)} = 0$. For $t \geq 1$, if $L^{(t)} - L_{opt} > 0$, we replace $L_{opt} = L^{(t)}$. Also, if $L^{(t)} - L_{opt} \leq \varepsilon L_{opt}$, we set $E^{(t)} = E^{(t-1)} + 1$. In this way, training continues as long as the improvement in the estimated lower bound in the validation set is greater than εL_{opt} , but if not, training is allowed to run for a set number of updates before early stopping. This leeway (called “*patience*”) is allowed due to the properties of stochastic gradient descent, which may cause $L^{(t)}$ to fluctuate, especially for smaller t . If $E^{(t)} = \textit{patience}$, we save the optimal model pertaining to L_{opt} , and terminate training. Here, we set *patience* = 50 and $\varepsilon = 0.0001$.

A2: Lower Bound with Known Covariate Distribution

In some cases, it may be more appropriate in *dlglm* to model the covariate distribution $p(\mathbf{X})$ with a known closed-form distribution, as described in Section 2.4.1 of the main text, rather

than the VAE/IWAE structure as described in Section 2.4.2 that is utilized by default in *dlglm*. Importantly, we no longer assume that the covariates \mathbf{X} are generated from some lower-dimensional latent variable \mathbf{Z} , as in a typical VAE/IWAE setting.

In this special case, a lower bound on the marginal log-likelihood in the presence of missingness can be computed as in Section 2.4.3. Under MNAR, this quantity, which we call \mathcal{L}_K^{dlglmX} , can be derived as

$$\begin{aligned}
\log p_{\alpha, \beta, \pi, \psi, \phi}(\mathbf{X}^o, \mathbf{Y}, \mathbf{R}^X) &= \sum_{i=1}^n \log p_{\alpha, \beta, \pi, \psi, \phi}(\mathbf{x}_i^o, y_i, \mathbf{r}_i^X) \\
&= \sum_{i=1}^n \log \left[\int p_{\alpha, \beta, \pi, \psi, \phi}(\mathbf{x}_i^o, \mathbf{x}_i^m, y_i, \mathbf{r}_i^X) d\mathbf{x}_i^m \right] \\
&= \sum_{i=1}^n \log \mathbb{E}_{\mathbf{x}_{ik}^m \sim q_{\theta}(\mathbf{x}_i^m | \mathbf{x}_i^o, \mathbf{r}_i^X, y_i)} \left[\frac{1}{K} \sum_{k=1}^K \frac{p_{\psi}(\mathbf{x}_i^o, \mathbf{x}_{ik}^m) p_{\alpha, \beta, \pi}(y_i | \mathbf{x}_i^o, \mathbf{x}_{ik}^m) p_{\phi}(\mathbf{r}_i^X | \mathbf{x}_i^o, \mathbf{x}_{ik}^m, y_i)}{q_{\theta}(\mathbf{x}_{ik}^m | \mathbf{x}_i^o, \mathbf{r}_i^X, y_i)} \right] \\
&\geq \sum_{i=1}^n \mathbb{E}_{\mathbf{x}_{ik}^m \sim q_{\theta}(\mathbf{x}_i^m | \mathbf{x}_i^o, \mathbf{r}_i^X, y_i)} \log \left[\frac{1}{K} \sum_{k=1}^K \frac{p_{\psi}(\mathbf{x}_i^o, \mathbf{x}_{ik}^m) p_{\alpha, \beta, \pi}(y_i | \mathbf{x}_i^o, \mathbf{x}_{ik}^m) p_{\phi}(\mathbf{r}_i^X | \mathbf{x}_i^o, \mathbf{x}_{ik}^m, y_i)}{q_{\theta}(\mathbf{x}_{ik}^m | \mathbf{x}_i^o, \mathbf{r}_i^X, y_i)} \right] = \mathcal{L}_K^{dlglmX}.
\end{aligned}$$

Similar to the default derivation of *dlglm*, we assume $\mathbf{x}_{i1}^m, \dots, \mathbf{x}_{iK}^m \stackrel{i.i.d}{\sim} q_{\theta}(\mathbf{x}_i^m | \mathbf{x}_i^o, \mathbf{r}_i^X, y_i)$, except now we have just the latent variables pertaining to the missing data, the weights and biases of the neural network that learns the variational posterior is now $\{\theta_1, \theta_2\} \rightarrow \theta$, and we need not specify a form for either the prior $p(\mathbf{z}_{ik})$ or the variational joint posterior which includes the latent variables pertaining to the lower-dimensional representation $\mathbf{z}_{i1}, \dots, \mathbf{z}_{iK}$. Instead, we assume an explicit covariate distribution $p_{\psi}(\mathbf{x}_i^o, \mathbf{x}_{ik}^m)$, which is indexed by some parameters ψ . For example, if $p_{\psi}(\mathbf{x}_i^o, \mathbf{x}_{ik}^m)$ is assumed to be distributed multivariate normal with an independent covariance structure, then $\psi = \{\boldsymbol{\mu}, \boldsymbol{\Sigma}\}$, where $\boldsymbol{\mu}$ is a mean vector of length p , and $\boldsymbol{\Sigma}$ is a $p \times p$ covariance matrix. One can then optimize values of ψ in conjunction with the weights and biases of the neural network architecture via stochastic gradient descent

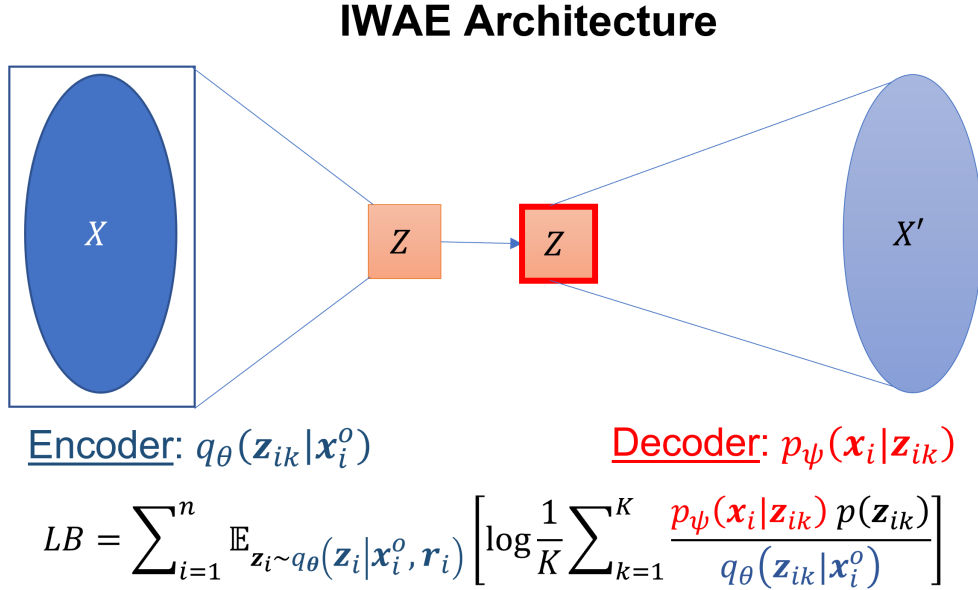
during training.

Also, the architecture would not contain the encoder $f_\psi(\mathbf{z}_i)$ and decoder $g_{\theta_1}(\mathbf{x}_i^o)$ neural networks as in Section 2.4.3, but would consist of the neural networks $g_\theta(\mathbf{x}_i^o, \mathbf{r}_i^X, y_i)$, $s_{\beta, \pi}(\mathbf{x}_i)$, and $h_\phi(\mathbf{x}_i, y_i)$, which would respectively output the parameters of $q_\theta(\mathbf{x}_i^m | \mathbf{x}_i^o, \mathbf{r}_i^X, y_i)$, $p(y_i | \mathbf{x}_i^o, \mathbf{x}_{ik}^m)$, and $p(\mathbf{r}_i^X | \mathbf{x}_i^o, \mathbf{x}_{ik}^m, y_i)$. Values of the missing entries will similarly be drawn from the $q_\theta(\mathbf{x}_i^m | \mathbf{x}_i^o, \mathbf{r}_i^X, y_i)$, whose parameters are output by the neural network $g_\theta(\mathbf{x}_i^o, \mathbf{r}_i^X, y_i)$, and the drawn values will be used as input for the downstream neural networks $s_{\beta, \pi}(\mathbf{x}_i)$ and $h_\phi(\mathbf{x}_i, y_i)$.

Under ignorable missingness, the analogous lower bound can be similarly obtained as in Section 2.4.3 for *idlgm* by assuming independence between the missing values \mathbf{X}^m and the missingness mask \mathbf{R}^X :

$$\mathcal{L}_K^{idlgmX} = \sum_{i=1}^n \mathbb{E}_{\mathbf{x}_{ik}^m \sim q_\theta(\mathbf{x}_i^m | \mathbf{x}_i^o, y_i)} \log \left[\frac{1}{K} \sum_{k=1}^K \frac{p_\psi(\mathbf{x}_i^o, \mathbf{x}_{ik}^m) p_{\alpha, \beta, \pi}(y_i | \mathbf{x}_i^o, \mathbf{x}_{ik}^m) p_\phi(\mathbf{r}_i^X | \mathbf{x}_i^o, y_i)}{q_\theta(\mathbf{x}_{ik}^m | \mathbf{x}_i^o, y_i)} \right]$$

A3: IWAE Architecture



Supplementary Figure 1: Architecture of an importance weighted autoencoder (IWAE) in the absence of missing data. Darkly colored nodes represent deterministic values, lightly colored nodes represent learned distributional parameters, and outlined (in red) nodes represent sampled values from learned distributions. Orange cells correspond to latent variables \mathbf{Z} . \mathbf{Z} is sampled K times from its posterior distribution. Below is the lower bound (LB), which is optimized via stochastic gradient descent.

A4: dlglm Training Algorithm

The training of the *dlglm* architecture proceeds as follows:

1. The missing entries are pre-imputed to zero and appended with observed entries, and fed into $g_{\theta_1}(\mathbf{x}_i^o)$, to learn parameters of $q_{\theta_1}(\mathbf{z}_i|\mathbf{x}_i^o)$.
2. K samples are drawn from $q_{\theta_1}(\mathbf{Z}|\mathbf{X}^o, \mathbf{R})$.
3. Samples from (2) are used as input for $f_{\psi}(\mathbf{z}_i)$, to learn the parameters of $p_{\psi}(\mathbf{x}_i|\mathbf{z}_i)$.
4. The samples from (2) are used again as input for $g_{\theta_2}(\mathbf{z}_i, \mathbf{r}_i^X, \mathbf{x}_i^o, y_i)$, concatenated with the observed data entries (with pre-imputed missing entries) the missingness mask,

and the response to learn parameters of $q_{\theta_2}(\mathbf{x}_i^m | \mathbf{z}_i, \mathbf{x}_i^o, \mathbf{r}_i^X, y_i)$.

5. We draw samples of \mathbf{x}_i^m from $q_{\theta_2}(\mathbf{x}_i^m | \mathbf{z}_i, \mathbf{x}_i^o, \mathbf{r}_i^X, y_i)$, and use them as input, concatenated with the response y_i and the fixed observed entries \mathbf{x}_i^o , into $h_\phi(\mathbf{x}_i, y_i)$ (or the mask decoder network) to learn the parameters associated with the model of the missingness mask $p_\phi(\mathbf{r}_i^X | \mathbf{x}_i, y_i)$.
6. We use the samples of \mathbf{x}_i^m from (5), concatenated with the observed variables \mathbf{x}_i^o as input into $s_{\beta, \pi}(\mathbf{x}_i)$ to output parameters of $p_{\alpha, \beta, \pi}(y_i | \mathbf{x}_i)$. The dispersion parameter α is additionally learned via stochastic gradient descent, along with the all of the weights and biases of the entire architecture.

Under simple distributional assumptions of $q_{\theta_2}(\mathbf{x}_i^m | \mathbf{z}_i, \mathbf{r}_i^X, \mathbf{x}_i^o, y_i)$, the sampling step in Step (5) is similar to the sampling of the latent variable \mathbf{Z} in Step (2), and both can be accomplished using the reparametrization trick (Kingma & Welling 2013). These steps outline the case where \mathbf{R}^X is independent on \mathbf{Z} .

A5: dlglm Case xy

In *dlglm*, Case xy is the most general type of missingness that can be encountered, where missingness is present in both the covariates \mathbf{X} , as well as the response \mathbf{Y} . In this case, one must additionally learn an approximate posterior distribution of the missing response \mathbf{Y}^m .

The dlglm bound can be derived similarly to the Case x missingness as follows:

$$\begin{aligned}
\log p_{\alpha,\pi,\psi,\phi}(\mathbf{X}^o, \mathbf{Y}^o, \mathbf{R}) &= \sum_{i=1}^n \log p_{\alpha,\pi,\psi,\phi}(\mathbf{x}_i^o, y_i^o, \mathbf{r}_i) \\
&= \sum_{i=1}^n \log \left[\iiint p_{\alpha,\pi,\psi,\phi}(\mathbf{x}_i^o, \mathbf{x}_i^m, y_i^o, y_i^m, \mathbf{r}_i^X, r_i^Y, \mathbf{z}_i) d\mathbf{z}_i d\mathbf{x}_i^m dy_i^m \right] \\
&= \sum_{i=1}^n \log \mathbb{E}_{(\mathbf{z}_{ik}, \mathbf{x}_{ik}^m, y_{ik}^m) \sim q_{\theta}(\mathbf{z}_i, \mathbf{x}_i^m, y_i^m)} \left[\frac{1}{K} \sum_{k=1}^K \frac{p_{\alpha,\pi,\psi,\phi}(\mathbf{x}_i^o, \mathbf{x}_{ik}^m, y_i^o, y_{ik}^m, \mathbf{r}_i^X, r_i^Y, \mathbf{z}_{ik})}{q_{\theta}(\mathbf{z}_{ik}, \mathbf{x}_{ik}^m, y_{ik}^m)} \right] \\
&\geq \sum_{i=1}^n \mathbb{E}_{(\mathbf{z}_{ik}, \mathbf{x}_{ik}^m, y_{ik}^m) \sim q_{\theta}(\mathbf{z}_i, \mathbf{x}_i^m, y_i^m)} \log \left[\frac{1}{K} \sum_{k=1}^K \frac{p_{\alpha,\pi,\psi,\phi}(\mathbf{x}_i^o, \mathbf{x}_{ik}^m, y_i^o, y_{ik}^m, \mathbf{r}_i^X, r_i^Y, \mathbf{z}_{ik})}{q_{\theta}(\mathbf{z}_{ik}, \mathbf{x}_{ik}^m, y_{ik}^m)} \right] \\
&= \mathcal{L}_K^{dlglm}, \tag{1}
\end{aligned}$$

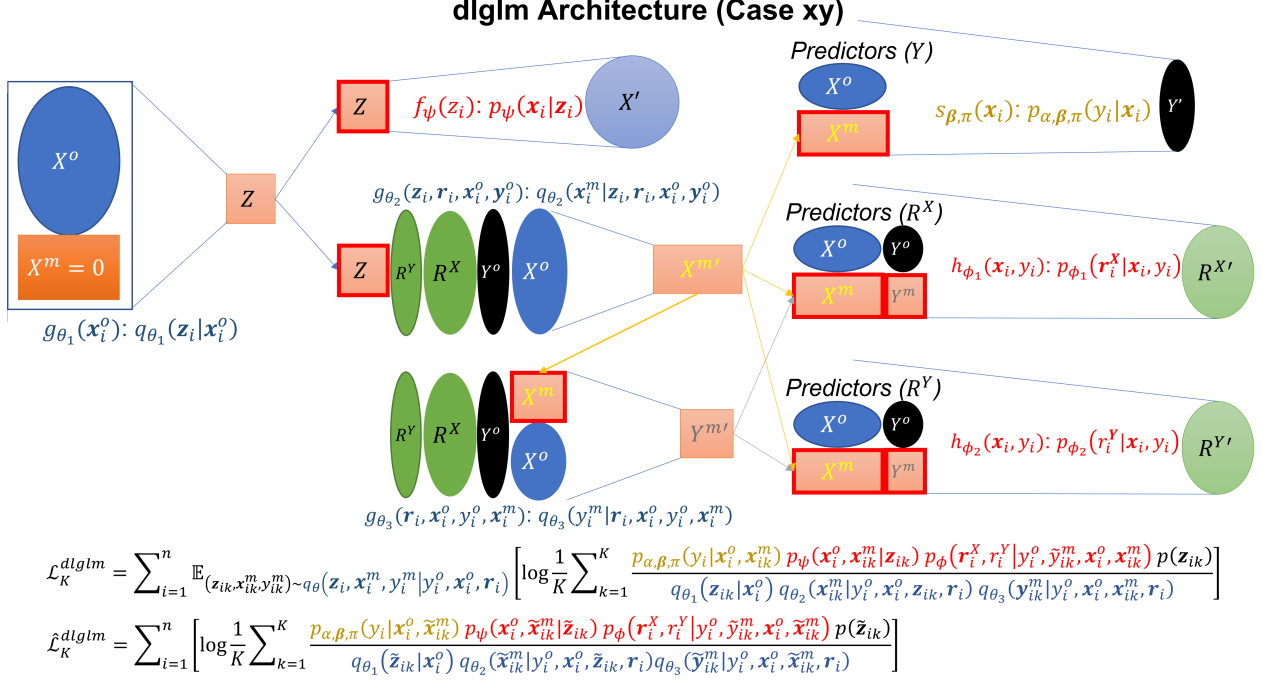
where now, we modify the factorization of the joint posterior as

$$q_{\theta}(\mathbf{Z}, \mathbf{X}^m, \mathbf{Y}^m) = q_{\theta_1}(\mathbf{Z}|\mathbf{X}^o)q_{\theta_2}(\mathbf{X}^m|\mathbf{Z}, \mathbf{X}^o, \mathbf{R})q_{\theta_3}(\mathbf{Y}^m|\mathbf{X}^o, \mathbf{X}^m, \mathbf{R}).$$

Then, the estimated dlglm bound is

$$\hat{\mathcal{L}}_K^{dlglm} = \sum_{i=1}^n \log \left[\frac{1}{K} \sum_{k=1}^K \frac{p_{\alpha,\psi}(y_i|\mathbf{x}_i^o, \tilde{\mathbf{x}}_{ik}^m)p_{\pi}(\mathbf{x}_i|\tilde{\mathbf{z}}_{ik})p(\tilde{\mathbf{z}}_{ik})p_{\phi_1}(\mathbf{r}_i|y_i^o, \tilde{y}_{ik}^m, \mathbf{x}_i^o, \tilde{\mathbf{x}}_{ik}^m)}{q_{\theta_1}(\tilde{\mathbf{z}}_{ik}|\mathbf{x}_i^o)q_{\theta_2}(\tilde{\mathbf{x}}_{ik}^m|\tilde{\mathbf{z}}_{ik}, \mathbf{x}_i^o, y_i^o, \mathbf{r}_i)q_{\theta_3}(\tilde{y}_{ik}^m|\mathbf{x}_i^o, \tilde{\mathbf{x}}_{ik}^m, y_i^o, \mathbf{r}_i)} \right]. \tag{2}$$

A visualization of the *dlglm* architecture in Case xy can be found in Figure 2.



Supplementary Figure 2: Architecture of proposed dlglm method (*Case xy*). Dark colored nodes ($X^o, X^m = 0, R^X, R^Y, Y^o$) represent deterministic values, lightly colored nodes ($Z, X^o, X^m, R^X, R^Y, Y^o$) represent learned distributional parameters, and outlined (in red) nodes represent sampled values. Orange cells correspond to latent variables \mathbf{Z}, \mathbf{X}^m , and \mathbf{Y}^m . $\mathbf{Z}_1, \dots, \mathbf{Z}_K, \mathbf{X}_1^m, \dots, \mathbf{X}_K^m$, and $\mathbf{Y}_1^m, \dots, \mathbf{Y}_K^m$ are sampled from their respective variational posteriors $q_{\theta_1}(\mathbf{Z} | \mathbf{X}^o)$, $q_{\theta_2}(\mathbf{X}^m | \mathbf{Z}, \mathbf{R}, \mathbf{X}^o, \mathbf{Y}^o)$, and $q_{\theta_3}(\mathbf{Y}^m | \mathbf{R}, \mathbf{X}^o, \mathbf{X}^m, \mathbf{Y}^o)$. Below is the dlglm bound (\mathcal{L}_K^{dlglm}), and the estimated dlglm bound ($\hat{\mathcal{L}}_K^{dlglm}$), which is optimized via stochastic gradient descent.

A6: Single Imputation via dlglm and idlglm

Following training, *dlglm* can also perform single imputation of missing values by obtaining point estimates for $\mathbb{E}[\mathbf{x}_i^m | \mathbf{x}_i^o, y_i, \mathbf{r}_i^X]$, defined as the expected value of the missing features given the observed data and the mask for the i^{th} observation under MNAR. We note that imputation is not the main focus of this paper, as it is primarily an unsupervised task, but it may be of interest in some settings to obtain these imputed values for downstream analyses.

To do this, we first note that

$$\begin{aligned}
\mathbb{E}[\mathbf{x}_i^m | \mathbf{x}_i^o, y_i, \mathbf{r}_i^X] &= \int \mathbf{x}_i^m p_{\alpha, \beta, \pi, \psi, \phi}(\mathbf{x}_i^m | \mathbf{x}_i^o, y_i, \mathbf{r}_i^X) d\mathbf{x}_i^m \\
&= \iint \mathbf{x}_i^m p_{\alpha, \beta, \pi, \psi, \phi}(\mathbf{x}_i^m, \mathbf{z}_i | \mathbf{x}_i^o, y_i, \mathbf{r}_i^X) d\mathbf{z}_i d\mathbf{x}_i^m \\
&= \iint \mathbf{x}_i^m \frac{p_{\alpha, \beta, \pi, \psi, \phi}(\mathbf{x}_i^m, \mathbf{x}_i^o, \mathbf{z}_i, y_i, \mathbf{r}_i^X)}{p_{\psi, \phi}(\mathbf{x}_i^o, y_i, \mathbf{r}_i^X)} d\mathbf{z}_i d\mathbf{x}_i^m.
\end{aligned}$$

Then, we can estimate this integral by self-normalized importance sampling. We utilize the proposal density $q_{\theta_1}(\mathbf{z}_i | \mathbf{x}_i^o) q_{\theta_2}(\mathbf{x}_i^m | \mathbf{z}_i, \mathbf{x}_i^o, y_i, \mathbf{r}_i^X)$, and define the quantities

$$w_{ik} = \frac{s_{ik}}{s_{i1} + \dots + s_{iK}}, \text{ and } s_{ik} = \frac{p_{\alpha, \beta, \pi}(y_i | \mathbf{x}_i^o, \tilde{\mathbf{x}}_i^m) p_{\psi}(\mathbf{x}_i | \tilde{\mathbf{z}}_{ik}) p(\tilde{\mathbf{z}}_{ik}) p_{\phi}(\mathbf{r}_i^X | \mathbf{x}_i^o, \tilde{\mathbf{x}}_{ik}^m, y_i)}{q_{\theta_1}(\tilde{\mathbf{z}}_{ik} | \mathbf{x}_i^o) q_{\theta_2}(\tilde{\mathbf{x}}_{ik}^m | \tilde{\mathbf{z}}_{ik}, \mathbf{x}_i^o, \mathbf{r}_i^X, y_i)}$$

for $k = 1, \dots, K$, with 1 sample drawn from the variational posterior of each latent variable \mathbf{z}_{ik} and \mathbf{x}_{ik}^m to compute s_{ik} , where w_{ik} is defined as standardized ‘‘importance weights’’ (Mattei & Frellsen 2019). Using these weights we may estimate $\mathbb{E}[\mathbf{x}_i^m | \mathbf{x}_i^o, y_i, \mathbf{r}_i^X] \approx \sum_{k=1}^K w_{ik} \tilde{\mathbf{x}}_{ik}^m$.

Then, the process can be repeated for each observation $i = 1, \dots, n$.

In the MCAR or MAR case, one can similarly estimate $\mathbb{E}[\mathbf{x}_i^m | \mathbf{x}_i^o, y_i]$ using the fitted *idlgm* model. By following a similar derivation using the proposal density $q_{\theta_1}(\mathbf{z}_i | \mathbf{x}_i^o) q_{\theta_2}(\mathbf{x}_i^m | \mathbf{z}_i, \mathbf{x}_i^o, y_i)$, we obtain the same approximation $\mathbb{E}[\mathbf{x}_i^m | \mathbf{x}_i^o, y_i] \approx \sum_{k=1}^K w_{ik} \tilde{\mathbf{x}}_{ik}^m$, with w_{ik} defined as before, but with a slightly different form for s_{ik} :

$$s_{ik} = \frac{p_{\alpha, \beta, \pi}(y_i | \mathbf{x}_i^o, \tilde{\mathbf{x}}_i^m) p_{\psi}(\mathbf{x}_i | \tilde{\mathbf{z}}_{ik}) p(\tilde{\mathbf{z}}_{ik})}{q_{\theta_1}(\tilde{\mathbf{z}}_{ik} | \mathbf{x}_i^o) q_{\theta_2}(\tilde{\mathbf{x}}_{ik}^m | \tilde{\mathbf{z}}_{ik}, \mathbf{x}_i^o, y_i)}.$$

Appendix B: Additional Details

B1: Tuning Hyperparameters

In this section, we summarize the combinations of hyperparameter values that were searched by *dlglm* and *idlglm*. For each dataset, we searched over combinations of two different values for each hyperparameter that was tuned. We tuned 4 different hyperparameters for each method: number of nodes per hidden layer (h), number of nodes per hidden layer in the missingness network (h_r), number of hidden layers (nhl), number of hidden layers in the $s_{\beta,\pi}(\mathbf{x}_i)$ network (nhl_y), number of hidden layers in the missingness network (nhl_r), dimensionality of latent space (dz), and learning rate (lr). For *idlglm*, $nhl_r = 0$ and $h_r = 0$ were fixed (since these are omitted in the *idlglm* architecture). Below are the searched values of the hyperparameters for each dataset in our analyses:

- Simulated Data ($p = \{25, 50\}$ features)
 - $h = \{128, 64\}$, $h_r = \{16, 32\}$
 - $lr = \{0.001, 0.01\}$
 - $dz = \{\lfloor 3 * p/4 \rfloor, \lfloor p/2 \rfloor, \lfloor p/4 \rfloor, \lfloor p/12 \rfloor\}$
 - $nhl = \{0, 1, 2\}$
 - $nhl_y = 0$
 - $nhl_r = \{0, 1\}$
 - $bs = 1,000$, $epochs_{max} = 2002$
- All UCI (including Banknote) datasets (p features)

- $h = \{128, 64\}$, $h_r = \{16, 32\}$
- $lr = \{0.001, 0.01\}$
- $dz = \{\lfloor 3 * p/4 \rfloor, \lfloor p/2 \rfloor, \lfloor p/4 \rfloor, 8\}$
- $nhl = \{0, 1, 2\}$
- $nhl_y = \{0, 1, 2\}$
- $nhl_r = \{0, 1\}$
- $bs = 1000$, $epochs_{max} = 2002$

B2: Additional Simulations

Supplementary Figures 3 and 4 show the results of the imputation, coefficient estimation, and prediction performance on simulated data with $p = 25$ fixed.

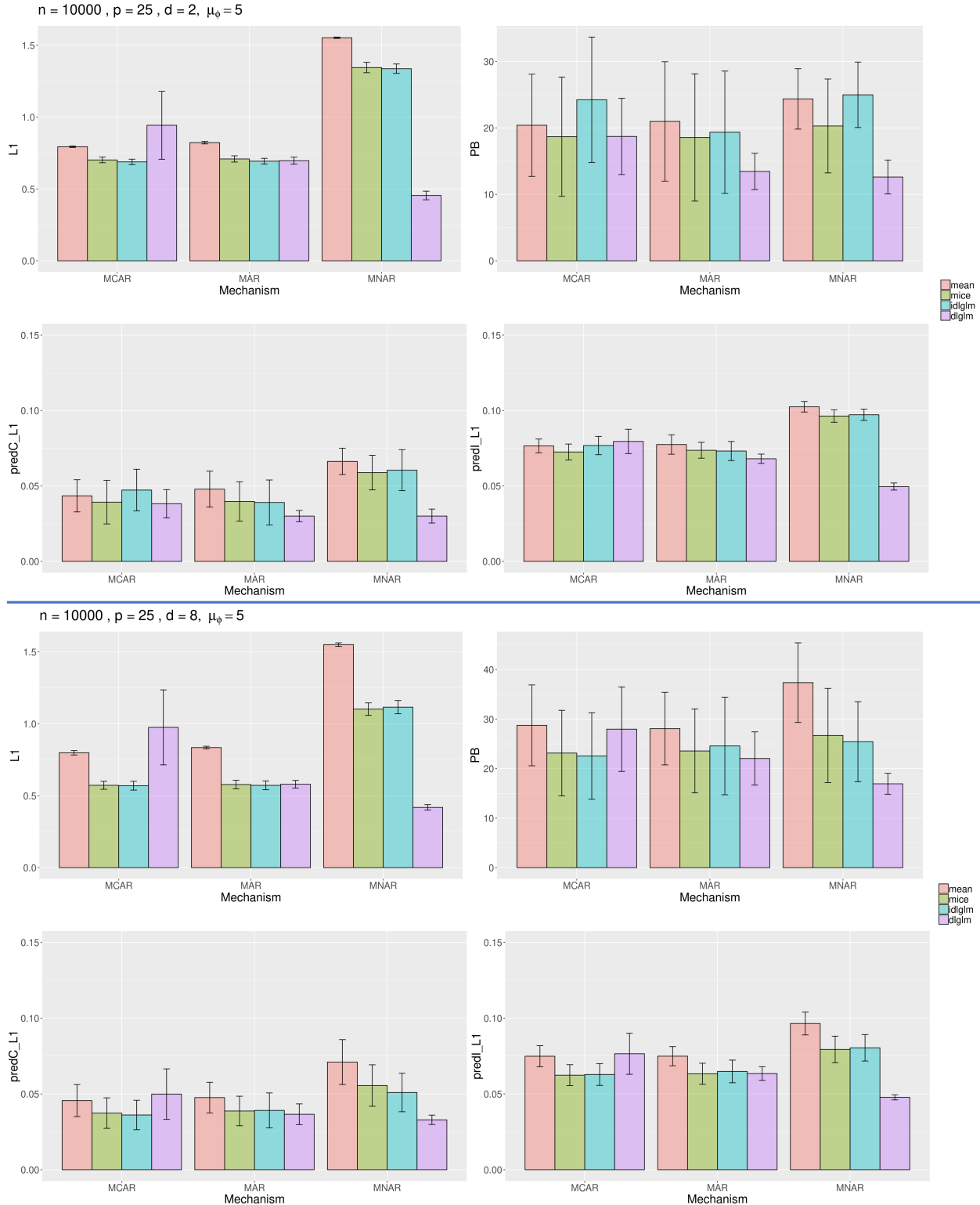
Appendix C: Data

Datasets used for analysis in this study are all publicly available online. Details of how to obtain these datasets are given in this section.

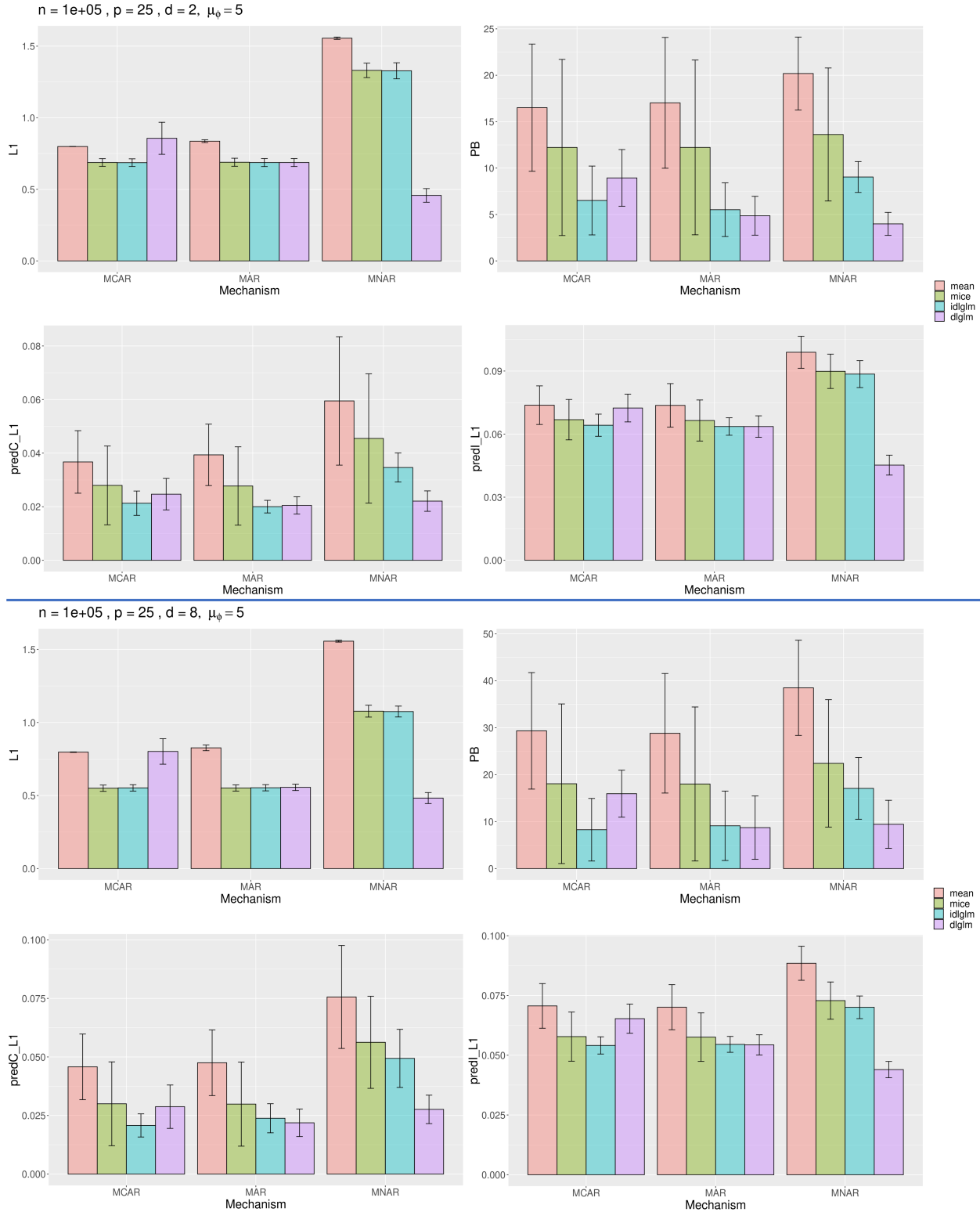
UCI Machine Learning Datasets

The UCI datasets can be obtained from the UCI Machine Learning repository at <https://archive.ics.uci.edu/ml/index.php> (Dua & Graff 2017) The datasets included in the analyses in this study (and in Appendix D) are given below:

1. CAREVALUATION: $n = 1728$ and $p = 6$.



Supplementary Figure 3: Simulation results with $n = 10,000$ and $p = 25$, varying $d = 2$ (top 4) and $d = 8$ (bottom 4). In each quadrant, we measure imputation accuracy by the average L1 distance between imputed vs true values in \mathbf{X} (top-left), coefficient estimation accuracy by the average percent bias (PB) of the estimates $\hat{\beta}$ compared to the truth (top-right), and prediction accuracy by the average L1 distance between the predicted and true probabilities of class 1 membership of \mathbf{Y} using the true unmasked test set (predC, bottom-left) and the incomplete test set (predI, bottom-right). In predI, we first impute missing values of the test data for mean and *mice* imputation, and we input the incomplete test set as is for *dlglm* and *idlglm*.



Supplementary Figure 4: Simulation results with $n = 100,000$ and $p = 25$, varying $d = 2$ (top 4) and $d = 8$ (bottom 4). In each quadrant, we measure imputation accuracy by the average L1 distance between imputed vs true values in \mathbf{X} (top-left), coefficient estimation accuracy by the average percent bias (PB) of the estimates $\hat{\beta}$ compared to the truth (top-right), and prediction accuracy by the average L1 distance between the predicted and true probabilities of class 1 membership of \mathbf{Y} using the true unmasked test set (predC, bottom-left) and the incomplete test set (predI, bottom-right). In predI, we first impute missing values of the test data for mean and *mice* imputation, and we input the incomplete test set as is for *dlglm* and *idlgm*.

- Documentation: <https://archive.ics.uci.edu/ml/datasets/car+evaluation>
- Link to Data: <https://archive.ics.uci.edu/ml/machine-learning-databases/car/car.data>
- Response of interest: Class variable (last feature)

2. BANKNOTE: $n = 1372$ and $p = 4$.

- Documentation: <https://archive.ics.uci.edu/ml/datasets/banknote+authentication>
- Link to Data: https://archive.ics.uci.edu/ml/machine-learning-databases/00267/data_banknote_authentication.txt
- Response of interest: Class variable (last feature)

3. DRYBEAN: $n = 13611$ and $p = 16$

- Documentation: <https://archive.ics.uci.edu/ml/datasets/Dry+Bean+Dataset>
- Link to Data: <https://archive.ics.uci.edu/ml/machine-learning-databases/00602/DryBeanDataset.zip>
- Response of interest: Class variable (last feature)

4. LETTER: $n = 20000$ and $p = 16$

- Documentation: <https://archive.ics.uci.edu/ml/datasets/letter+recognition>
- Link to Data: <https://archive.ics.uci.edu/ml/machine-learning-databases/letter-recognition/letter-recognition.data>
- Response of interest: Class variable (first feature)

5. RED: $n = 1599$ and $p = 11$

- Documentation: <https://archive.ics.uci.edu/ml/datasets/wine+quality>
- Link to Data: <https://archive.ics.uci.edu/ml/machine-learning-databases/wine-quality/winequality-red.csv>
- Response of interest: Wine quality score (last feature)

6. SHUTTLE: $n = 57756$ (after pre-filtering low-incidence classes) and $p = 9$

- Documentation: [https://archive.ics.uci.edu/ml/datasets/Statlog+\(Shuttle\)](https://archive.ics.uci.edu/ml/datasets/Statlog+(Shuttle))
- Link to Data: Attained using the *mlbench* R package, using the command:
`data(Shuttle)`
- Response of interest: Class variable (last feature)

7. SPAM: $n = 4601$ and $p = 57$

- Documentation: <https://archive.ics.uci.edu/ml/datasets/spambase>
- Link to Data: <https://archive.ics.uci.edu/ml/machine-learning-databases/spambase/spambase.data>
- Response of interest: Class variable (last feature)

8. WHITE: $n = 4898$ and $p = 11$

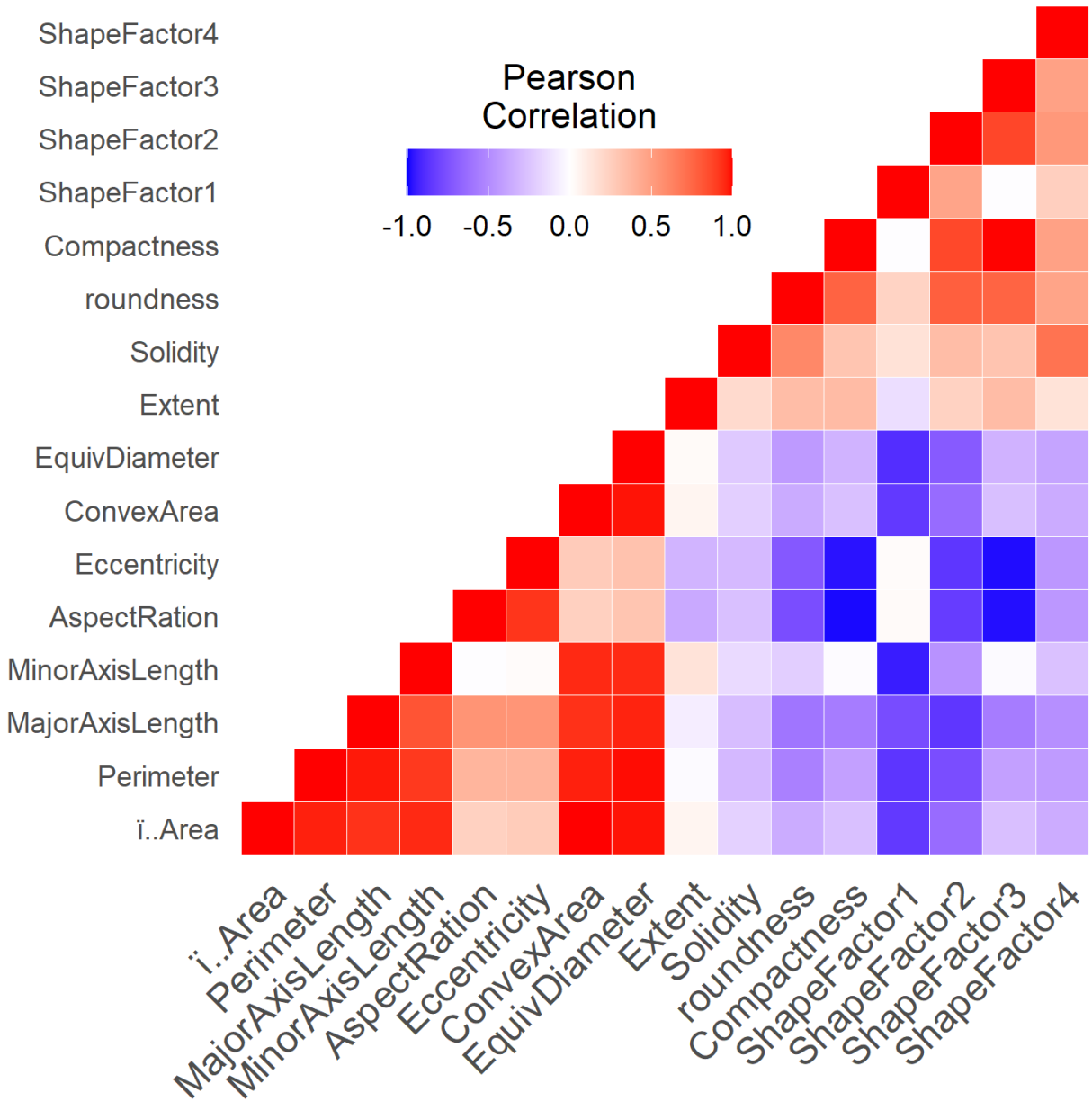
- Documentation: <https://archive.ics.uci.edu/ml/datasets/wine+quality>
- Link to Data: <https://archive.ics.uci.edu/ml/machine-learning-databases/wine-quality/winequality-white.csv>

- Response of interest: Wine quality score (last feature)

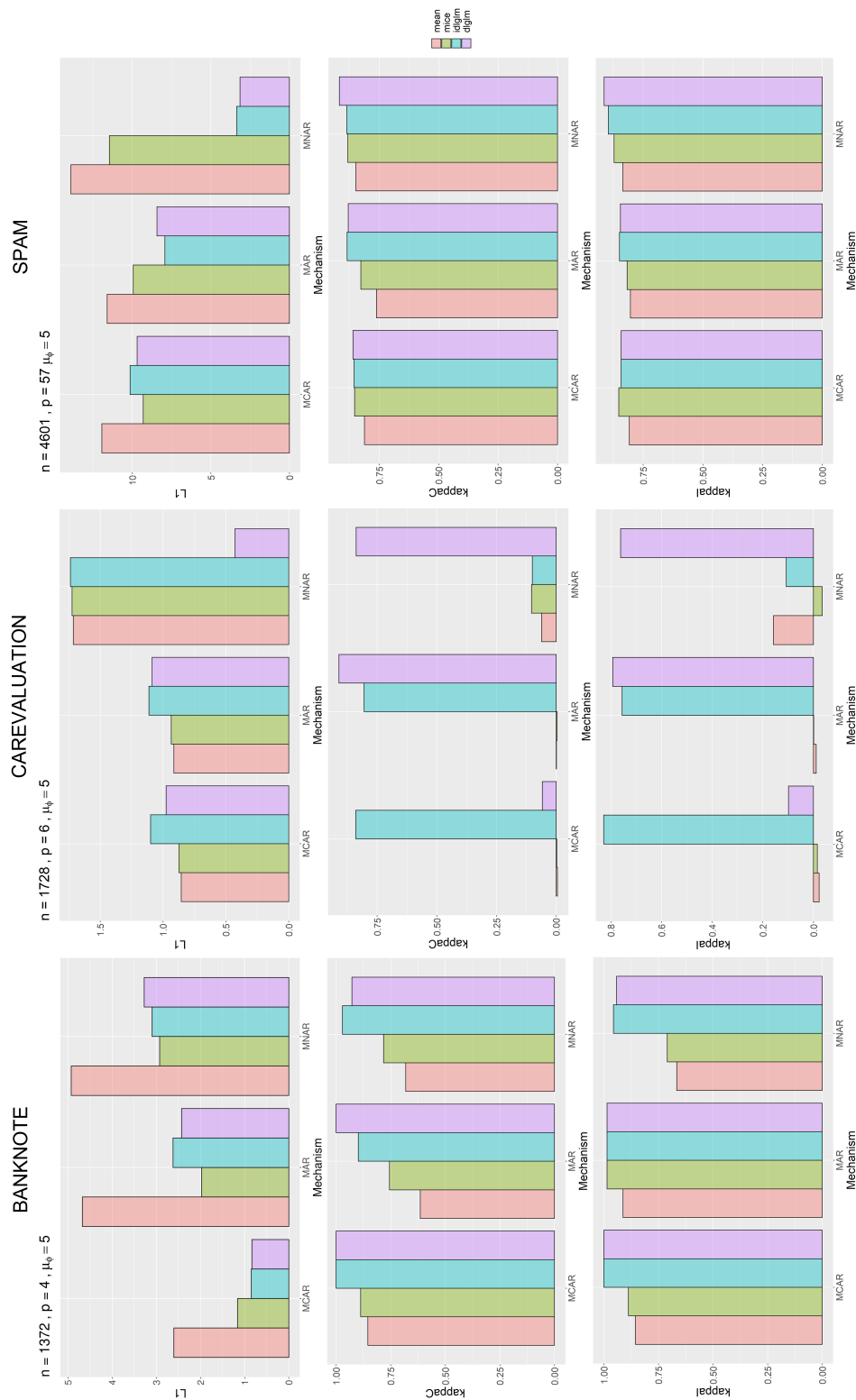
In particular, the DRYBEAN dataset contained very highly correlated features, as can be seen in the heatmap in Supplementary Figure 5. Such high correlation between features may allow ignorably-missing methods do perform well under non-ignorable missingness, as the partially-observed features that the missingness depends on may be highly correlated with completely-observed features in the dataset.

Appendix D: Additional Simulations

We also performed comparative analyses in 5 other small UCI datasets, as in Section 3.2 in the main text. Supplementary Figures 6 and 7 show the results for these analyses for the BANKNOTE, CAREVALUATION, SPAM, RED, and WHITE datasets. In general, we see that *dlglm* still performs best in imputation and prediction under MNAR missingness, although *idlglm* performs slightly better in the BANKNOTE dataset. In lower sample size settings, *dlglm* may not perform optimally, due to the more complex architecture and the additional task of learning a missingness model. We also note that for these missingness models in *dlglm*, as in the main text, we included all of the features in \mathbf{X} as well as the response variable \mathbf{Y} as covariates, although only one feature in \mathbf{X} is involved in the simulation of missingness in each incomplete feature. Selecting important features from an overparameterized missingness model may be very difficult, and thus we recommend *dlglm* to be used with a sample size of at least $n = 10000$.



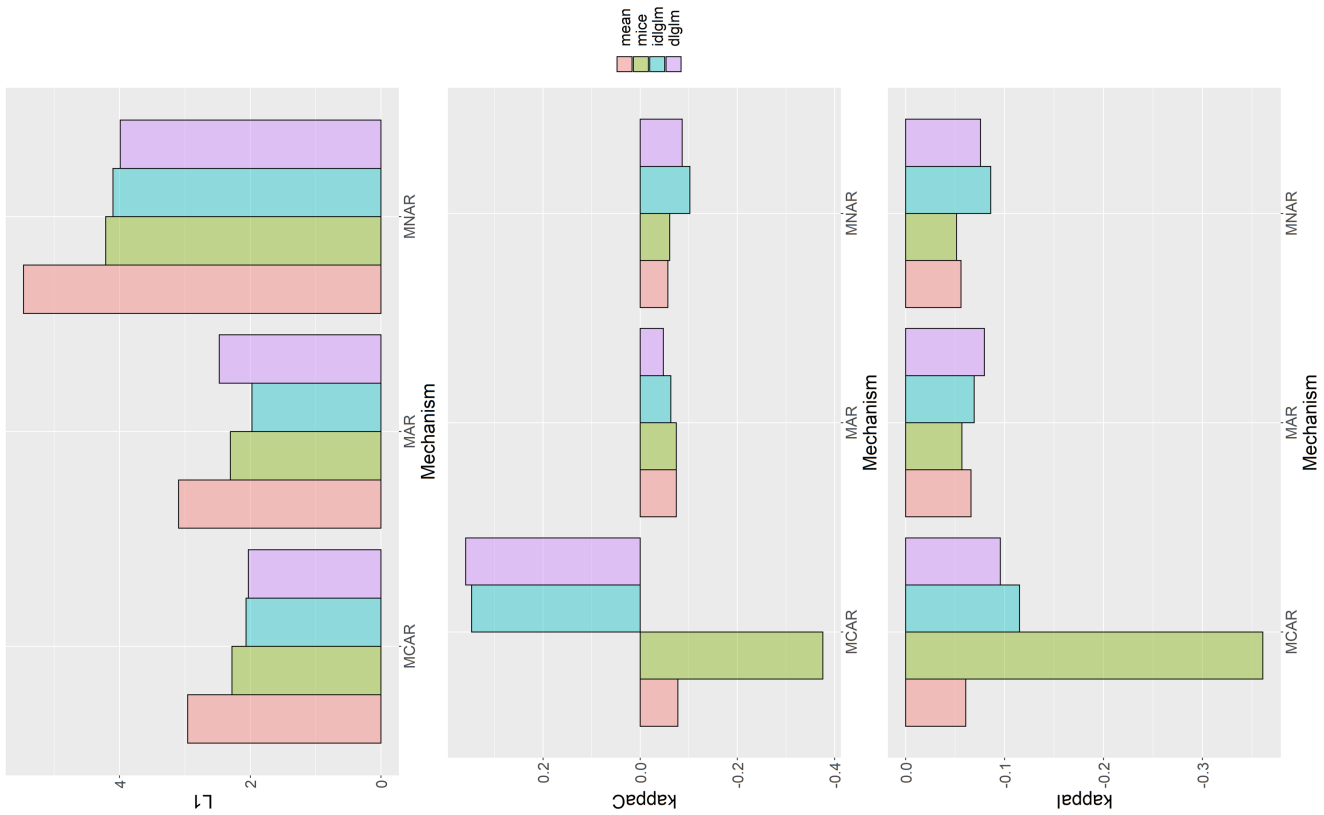
Supplementary Figure 5: Correlation heatmap matrix of features in the DRYBEAN dataset. Many features in this dataset were highly correlated.



Supplementary Figure 6: Imputation (top row) and prediction results from predC (middle row) and predI (bottom row) from comparative methods run on 3 small datasets from the UCI Machine Learning Repository: BANKNOTE, CAREVALUATION, and SPAM (columns, left to right). Imputation error was measured by the average L1 distance between true and imputed entries, with lower values indicating better performance, and prediction performance was measured by the Cohen's kappa metric for both predC (kappaC) and predI (kappaI), with higher values indicating better performance.

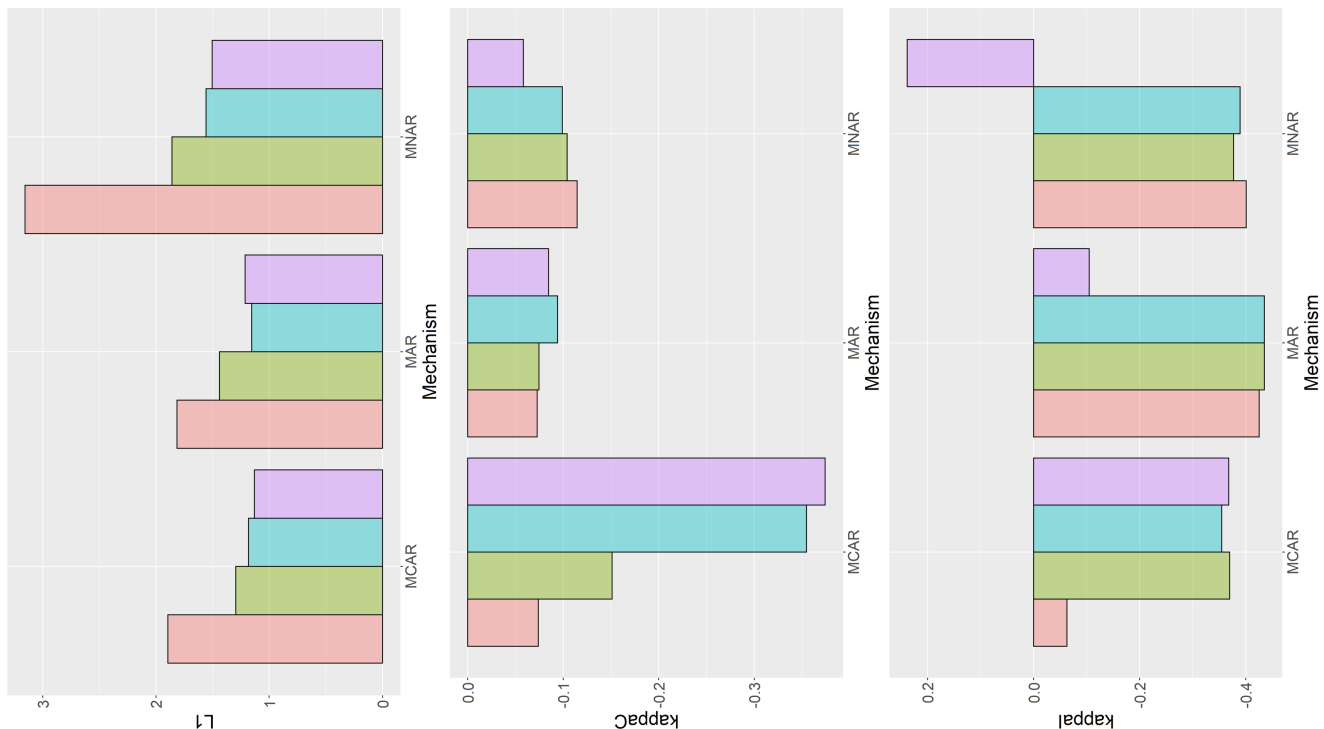
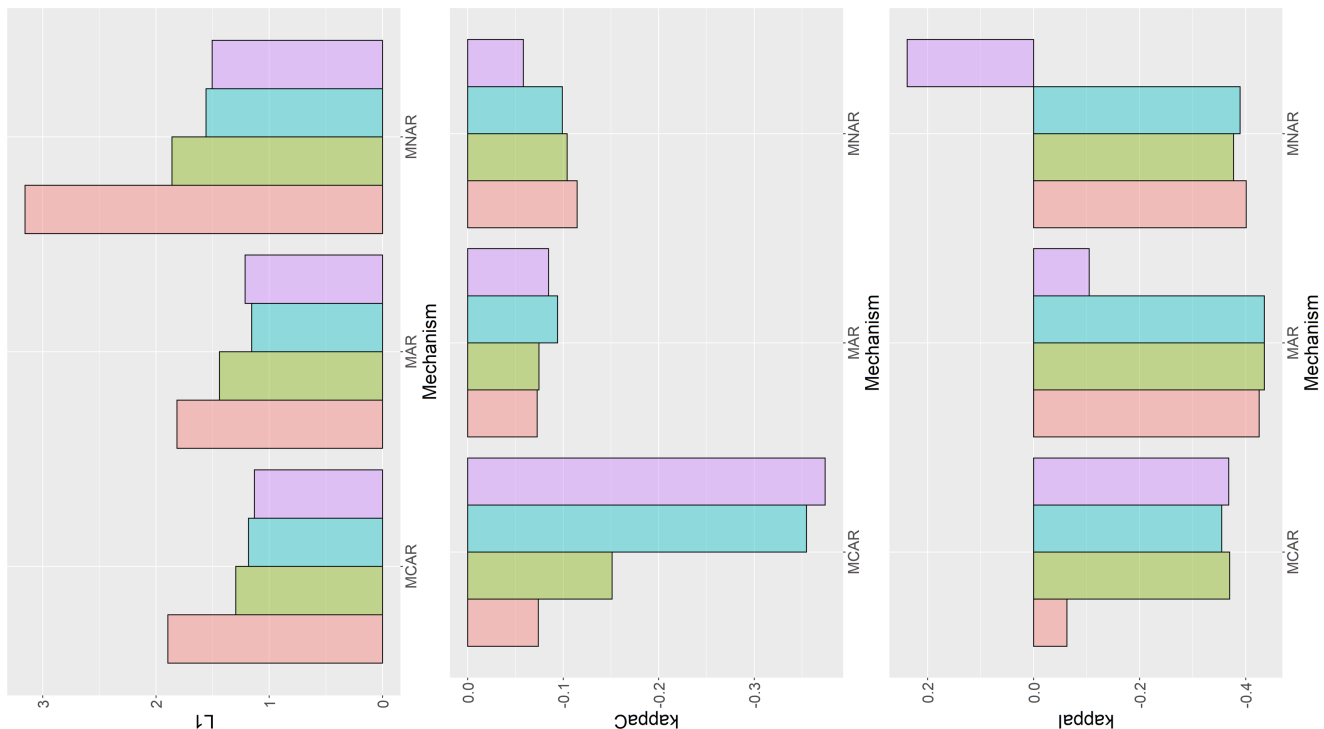
WHITE

$n = 4898, p = 11, \mu_0 = 5$



RED

$n = 1599, p = 11, \mu_0 = 5$



Supplementary Figure 7: Imputation (top row) and prediction results from predC (middle row) and predI (bottom row) from comparative methods run on 2 small datasets from the UCI Machine Learning Repository: RED and WHITE (columns, left and right). Imputation error was measured by the average L1 distance between true and imputed entries, with lower values indicating better performance, and prediction performance was measured by the Cohen's kappa metric for both predC (kappaC) and predI (kappaI), with higher values indicating better performance.

Appendix E: Bank Marketing Dataset

The Bank Marketing dataset contains 17 attributes collected from 41,188 clients from direct marketing campaigns of a Portuguese banking institution. The dataset is publicly available here: <https://archive.ics.uci.edu/ml/machine-learning-databases/00222/bank-additional.zip>. Any “unknown” or “nonexistent” values in the data were deemed to be missing. Also, a value of 999 for *pdays* (the number of days that passed by after the client was last contacted from a previous campaign) was denoted as missing. The response variable of interest was a binary indicator of whether the client subscribed to the term deposit. We omitted the month and day of the call due to irrelevance with respect to the response variable. We also removed the call duration variable as stated in the documentation, due to a strong correlation with the response. The resulting dataset contained 16 features for each of the 41,188 clients. More information about this dataset can be found in <https://archive.ics.uci.edu/ml/datasets/bank+marketing>.

References

- Boyd, S., Parikh, N., Chu, E., Peleato, B., Eckstein, J. et al. (2011), ‘Distributed optimization and statistical learning via the alternating direction method of multipliers’, *Foundations and Trends® in Machine learning* **3**(1), 1–122.
- Dua, D. & Graff, C. (2017), ‘UCI machine learning repository’.
- URL:** <http://archive.ics.uci.edu/ml>

- Jang, E., Gu, S. & Poole, B. (2016), ‘Categorical reparameterization with gumbel-softmax’, *arXiv preprint arXiv:1611.01144* .
- Kingma, D. P. & Ba, J. (2014), ‘Adam: A Method for Stochastic Optimization’, *arXiv e-prints* p. arXiv:1412.6980.
- Kingma, D. P. & Welling, M. (2013), ‘Auto-Encoding Variational Bayes’, *arXiv e-prints* p. arXiv:1312.6114.
- Lydia, A. & Francis, S. (2019), ‘Adagrad—an optimizer for stochastic gradient descent’, *Int. J. Inf. Comput. Sci* **6**(5), 566–568.
- Mattei, P.-A. & Frellsen, J. (2019), MIWAE: Deep generative modelling and imputation of incomplete data sets, *in* K. Chaudhuri & R. Salakhutdinov, eds, ‘Proceedings of the 36th International Conference on Machine Learning’, Vol. 97 of *Proceedings of Machine Learning Research*, PMLR, Long Beach, California, USA, pp. 4413–4423.
- Prechelt, L. (1998), Early stopping-but when?, *in* ‘Neural Networks: Tricks of the trade’, Springer, pp. 55–69.
- Saxe, A. M., McClelland, J. L. & Ganguli, S. (2014), Exact solutions to the nonlinear dynamics of learning in deep linear neural network, *in* ‘In International Conference on Learning Representations’.
- Tran, M.-N., Nguyen, N., Nott, D. & Kohn, R. (2019), ‘Bayesian deep net GLM and GLMM’, *Journal of Computational and Graphical Statistics* **29**(1), 97–113.